Application of the Coherent Potential Approximation to the Excited Electronic States of Substitutionally Disordered Molecular Crystals

JOSEPH HOSHEN AND JOSHUA JORTNER
Department of Chemistry, Tel-Aviv University, Tel-Aviv, Israel
(Received 29 October 1971)

In this paper we apply the coherent potential approximation for the calculation of the density of excited electronic states and of the optical properties of a variety of isotopically mixed molecular crystals where the pure crystal exciton band structure and density of state is determined by one, two, and three dimensional interactions. The crystal Hamiltonian is characterized by a random diagonal part and by a translationally invariant off diagonal part. Numerical results are provided for the following systems:

(a) a one dimensional chain in the amalgamation limit, in the persistence case and in the separated bands limit;
(b) the lowest triplet state of naphthalene in the separated bands case;
(c) the lowest singlet state of naphthalene in the amalgamation limit, in the persistence case and in the separated bands limit.
(d) The lowest singlet state of benzene in the persistence case and in the separated bands limit.

These calculations demonstrated the general features of the density of states in substitutionally disordered crystals, such as the erosion of the Van Hove singularities in the band(s), and the nature of the intensity distribution such as number of Davydov components, their relative intensities, location, and widths. The predictions of the CPA for the moments of the density of states and for the optical properties concur with the predictions of the general moment expansion method for a configurationally averaged crystal. A general CPA scheme is provided to handle tertiary mixed crystals, which are of some experimental interest. To account for the concentration dependence of the optical properties of isotopically mixed benzene, we provide a semiquantitative extension of the CPA scheme, where the isotope effect on the environmental shift term is incorporated into the virtual crystal Hamiltonian resulting in concentration dependent diagonal terms in the crystal Hamiltonian.

I. INTRODUCTION

Experimental and theoretical studies of the excited electronic states of mixed molecular crystals[1–10] are of considerable current interest for the understanding of the electronic structure of disordered systems. Isotopically mixed molecular crystals provide a prototype for the study of substitutionally disordered solids, where the two components just differ in the diagonal matrix elements of the Hamiltonian.[4,7–10] In a recent work we have presented a systematic study of this problem.[10] The general features of the excited electronic states of an isotopically substituted crystal can be elucidated by invoking a single hypothesis of complete random distribution of the molecules on the lattice sites.[10–13] Thus one can define[11] an effective Hamiltonian determined only by the concentration and by the strength of the random perturbation. The low moments of the density of excited states[11] and of the intensity distribution in optical absorption[10] can be expressed in terms of the density of states and the energies of the Davydov components in the pure crystal. The general properties of the complex effective Hamiltonian or rather the complex self-energy determine the conditions for the appearance of a bandgap in the density of states[10–13] and determine the number of the Davydov components in the mixed crystal.[7–10] In order to obtain an explicit theoretical expression for the self-energy, the coherent potential approximation (CPA) is then introduced.[11–13] The CPA invokes the hypothesis that multiple scattering effects are negligible.[11–13] The CPA exhibits some very satisfactory features,[6–13] i.e., it is symmetric in the concentration of the two components; it provides a faithful reproduction of exact results in various limiting cases, such as the low concentration limit, the virtual crystal limit, and the atomic limit (which is equivalent[10] to the Rashba–Broude[3] scheme).

In this paper we present the results of numerical calculations on the excited electronic states of mixed molecular crystals, based on the CPA, for a number of model systems. We shall handle a one dimensional model system where analytical expressions for the self-energy can be provided. Then we proceed to treat a two dimensional system which is applicable to triplet exciton states in some heavily mixed aromatic crystals. In the calculations for one and two dimensional systems we have utilized the explicit form of the exciton transfer integrals for the calculation of the pure crystal density of states. Perhaps the most attractive feature of the CPA is that only directly accessible experimental data which are the pure crystal density of states and the positions of the Davydov components are required for the calculation of the properties of the mixed crystals. For the case of a three dimensional system we have investigated the lowest singlet state of isotopically mixed naphthalene and benzene crystals, these calculations being somewhat more elaborate than those previously performed by Hong and Robinson[7,9] and by us[8] for the case of napthalene. The calculations

presented herein demonstrate some general features of the density of states of substitutionally disordered organic crystals, such as the erosion of the Van Hove singularities, and establish the characteristics of the intensity distribution in absorption. Finally, the general study was extended to handle the properties of tertiary mixed crystals, which are of some experimental interest.

II. A CONFIGURATIONALLY AVERAGED MIXED CRYSTAL

In what follows we shall use the same definitions and adopt the notation previously used by us[10] to describe the excited electronic states of a substitutionally mixed crystal consisting of two components A (concentration C_A) and B (concentration C_B). The crystal Hamiltonian can be recast in the form

$$H=H_0+H_1, \tag{II.1}$$

where the virtual crystal Hamiltonian H_0 is given by

$$H_0=\sum_n\sum_\alpha |\, n\alpha\rangle\tilde{\epsilon}\langle n\alpha\,|+J, \tag{II.2}$$

while the mean single molecule excitation energy in the crystal is

$$\tilde{\epsilon}=C_A(\Delta\epsilon_A{}^f+D^f)+C_B(\Delta\epsilon_B{}^f+D^f)\equiv C_A\epsilon_A+C_B\epsilon_B. \tag{II.3}$$

Here $|\, n\alpha\rangle$ labels a localized excitation wavefunction at the crystal site $n\alpha$, $n=1\cdots N$ is the number of unit cells, while $\alpha=1\cdots\sigma_D$ labels the molecules in the unit cell, $\Delta\epsilon_A{}^f$ and $\Delta\epsilon_B{}^f$ represent the free molecules excitation energies, D^f is the environmental shift term, and $\epsilon_{A,B}=\Delta\epsilon_{A,B}{}^f+D^f$; J is the crystal excitation transfer operator. It is explicitly assumed that both D^f and J are invariant under isotopic substitution. The deviation of the crystal Hamiltonian from the virtual crystal is

$$H_1=\Delta\sum_n\sum_\alpha |\, n\alpha\rangle\xi_{n\alpha}\langle n\alpha\,|, \tag{II.2'}$$

where $\xi_{n\alpha}$ is a random variable so that $\xi_{n\alpha}=-C_A$ when site $n\alpha$ is occupied by B, while $\xi_{n\alpha}=C_B$ when this site is occupied by A. The quantity $\Delta=\Delta\epsilon_A{}^f-\Delta\epsilon_B{}^f\equiv\epsilon_A-\epsilon_B$ represents the difference in the molecular excitation energies.

Now, assuming that molecule–molecule spatial correlations can be neglected,[11–13] the physical properties of the mixed crystal can be described by the configurationally averaged Green's function $\langle G(z)\rangle$ given by

$$\langle G(z)\rangle=\langle 1/(z-H)\rangle=1/(z-H_{\rm eff}). \tag{II.4}$$

Equation (II.4) defines the effective Hamiltonian $H_{\rm eff}$, which characterizes the properties of the averaged crystal and which can be expressed in terms of the complex self-energy $\Sigma(z)$ of mixed crystal with respect to the virtual crystal

$$H_{\rm eff}(z)=H_0+\Sigma(z). \tag{II.5}$$

The density (per molecule) of excited states $\rho(E)$ for a mixed crystal where the molecules in the unit cell are crystallographically invariant can be expressed in the form

$$\rho(E)=(1/\pi N\sigma_D)\ \mathrm{Im}\,\mathrm{Tr}\langle G(z)\rangle$$
$$=(1/\pi)\ \mathrm{Im}\langle n\alpha\,|\,\langle G(E-i0^+)\rangle\,|\,n\alpha\rangle. \tag{II.6}$$

In a manner formally equivalent to the Koster–Slater scheme[11,14] one can define a complex function

$$f(z)=(N\sigma_D)^{-1}\,\mathrm{Tr}\langle G(z)\rangle=\int_{-\infty}^{\infty}\frac{dE'}{z-E'}\,\rho(E') \tag{II.7}$$

so that the density of states is

$$\rho(E)=\pi^{-1}\,\mathrm{Im}f(E-i0^+). \tag{II.8}$$

To describe the optical properties of the mixed crystal, we shall describe the dipole strength $I_j(E)$ for polarized light absorption to the jth excitation branch ($j=1\cdots\sigma_D$) in terms of the $\mathbf{k}=0$ component of the spectral density function[11] $S(\mathbf{k}, j, E)$ corresponding to that particular excitation branch, so that[10]

$$I_j(E)=|\,m(j)\,|^2S(0,j,E), \tag{II.9}$$

where

$$S(\mathbf{k},j,E)=\pi^{-1}\,\mathrm{Im}\langle\mathbf{k}j\,|\,\langle G(E-io^+)\rangle\,|\,\mathbf{k}j\rangle \tag{II.10}$$

is just the diagonal matrix element of the configurationally averaged Green's function (below the complex plane) in the $|\,\mathbf{k}j\rangle$ delocalized exciton representation. Finally, $m(j)$ represents the transition moment for the jth pure (or virtual) crystal exciton branch.

Without referring to any specific approximations the following general results can be derived for the configurationally averaged crystal[10–13]:

(a) Some necessary conditions for the appearance of an energy gap in the density of states can be formulated. Four physical situations can be distinguished:

(a^1) Separated bands, whereupon a forbidden energy region which is simultaneously forbidden for the states of the pure crystals A and B, will appear between the two bands in the mixed crystal. This situation will be realized when the perturbation strength Δ exceeds the total bandwidth W of the pure crystal

$$|\,\Delta\,|>W. \tag{II.11}$$

(a^2) The persistence case is characterized by a nearly forbidden energy region inside the region spanned by the two bands of the pure components. General arguments lead to the following condition for this case:

$$W^2\geq C_AC_B\Delta^2\geq\mu_2{}^0, \tag{II.12}$$

where $\mu_2{}^0$ is the second moment of the density of states of the pure crystal.

(a^3) An incipient band gap will be exhibited when

$$\mu_2{}^0\gtrsim C_AC_B\Delta^2 \tag{II.13}$$

providing an intermediate situation between cases (a^2) and (a^4).

(a[4]) The amalgamation limit will be realized when

$$\Delta^2 < \mu_2^0 \ll W \tag{II.14}$$

and one band exists in the density of states function. In this limit the electronic states of the crystal can be reasonably well characterized by the virtual crystal Hamiltonian.

(b) The moments μ_p of the density of states and the moments $M_p(\mathbf{k}, j)$ of the spectral density can be expressed in the general form[10,11]

$$\mu_p = \int dE \rho(E) E^p = (1/N\sigma_D)\ \mathrm{Tr}\langle H^p \rangle, \tag{II.15a}$$

$$M_p(\mathbf{k}, j) = \int dE S(\mathbf{k}, j, E) E^p = \langle \mathbf{k}j \mid \langle H^p \rangle \mid \mathbf{k}j \rangle \tag{II.15b}$$

leading to explicit expressions for the moments of the mixed crystal in terms of the moments of the density of states of the pure crystal, the energy dispersion relation for the pure crystal, the perturbation strength Δ, and the concentrations of the constituents[10,11]:

$$\mu_0 = 1,$$
$$\mu_1 = \tfrac{1}{2}\Delta(C_A - C_B),$$
$$\mu_2 = \mu_2^0 + \Delta^2/4. \tag{II.16a}$$

The moments $N_p(j)$ of the polarized absorption bands can be expressed in the form

$$N_p(j) = \mid m(j) \mid^2 M_p(0, j) \tag{II.17}$$

where M_p is given by (II.16).

(c) In the case of separated bands and in the persistence case we can consider[10,11] two separate subbands which will be labeled by α and β so that the density of states and the spectral density functions can now be decomposed in the following form: $\rho(E) = \rho^\alpha(E) + \rho^\beta(E)$ and $S(\mathbf{k}, j, E) = S^\alpha(\mathbf{k}, j, E) + S^\beta(\mathbf{k}, j, E)$. The moments of the density of states in the two subbands can be expressed (up to second order in Δ^{-1}) in the form[10,11]

$$\mu_0^\alpha = C_A, \qquad \mu_0^\beta = C_B;$$
$$\mu_1^\alpha = C_A C_B \mu_2^0/\Delta, \qquad \mu_1^\beta = C_A C_B \mu_2^0/\Delta;$$
$$\mu_2^\alpha = C_A^2 \mu_2^0, \qquad \mu_2^\beta = C_B^2 \mu_2^0. \tag{II.16b}$$

From the general expressions obtained for the moments of the spectral density the following results can be derived for the optical properties of the mixed crystal[8]:

(c[1]) When a gap exists in the density of states, we can expect $2\sigma_D$ different intensity distributions in the binary mixed crystal. In the region of each subband σ_D polarized intensity distributions will be exhibited.

(c[2]) The relative integrated intensities $A^\alpha(j)$ and $A^\beta(j)$ of the absorption bands are[10]

$$A^\alpha(j) = \mid m(j) \mid^2 [C_A + 2C_A C_B t_j \Delta^{-1} - 3C_B(C_A - C_B) \times (t_j^2 - \mu_2^0)\Delta^{-2} + O(\Delta^{-3})],$$
$$A^\beta(j) = \mid m(j) \mid^2 [C_B - 2C_A C_B t_j \Delta^{-1} + 3C_A(C_B - C_A) \times (t_j^2 - \mu_2^0)\Delta^{-2} + O(\Delta^{-3})], \tag{II.18}$$

where t_j is the energy of the jth Davydov component (measured relative to the energy $\Delta\epsilon_A{}^f + D^f \equiv \epsilon_A$) in the pure crystal.

(c[3]) The centers of gravity $E_c^\alpha(j)$ and $E_c^\beta(j)$ of the optical absorption bands can be expressed in terms of the interpolation formula[10]:

$$E_c^\alpha(j) = \epsilon_A + C_A t_j + C_A C_B t_j^2 \Delta^{-1} - 3C_A C_B \mu_2^0 \Delta^{-1} + C_B \mu_2^0 \Delta^{-1} + O(\Delta^{-2}),$$
$$E_c^\beta(j) = \epsilon_B + C_B t_j - C_A C_B t_j^2 \Delta^{-1} + 3C_A C_B \mu_2^0 \Delta^{-1} - C_A \mu_2^0 \Delta^{-1} + O(\Delta^{-2}). \tag{II.19}$$

We should note in passing that these results provide the "deep trap" energy values $E_c^{\alpha,\beta}(j) = \Delta\epsilon_{A,B} + D^f \pm \mu_2^0 \Delta^{-1}$ in the zero concentration limit.

(c[4]) The standard deviation $Y^\alpha(j)$ and $Y^\beta(j)$ for the intensity distributions are given by[10]

$$Y^\alpha(j) = Y^\beta(j) = (C_A C_B \mu_2^0)^{1/2} + O(\Delta^{-1}). \tag{II.20}$$

(d) In the amalgamation case the following features of the intensity distribution are exhibited:

(d[1]) σ_D intensity distributions are revealed, their number being thus equal to that of the Davydov components in the pure crystal.

(d[2]) The integrated intensity of each absorption band is equal to that of the corresponding Davydov component in the pure crystal[10]

$$A(j) = \mid m(j) \mid^2. \tag{II.21}$$

(d[3]) The center of gravity of each intensity distribution corresponds to the position of the Davydov component in the virtual crystal[10]

$$E_c(j) = C_A \epsilon_A + C_B \epsilon_B + t_j = \tilde{\epsilon} + t_j. \tag{II.22}$$

(d^4) The width of each intensity distribution is independent of the excitation branch being[10]

$$Y(j) = \mid \Delta \mid (C_A C_B)^{1/2}. \tag{II.23}$$

One should notice that unlike the approximate results derived for the case of separated bands which are determined by a power series $\sim\Delta^{-1}$, the expressions for the amalgamation limit are exact.

Up to this point we have considered the general properties of the configurationally averaged crystal. To proceed, a further approximation has to be invoked involving the local nature of the self-energy operator, which in the localized representation is assumed to take

the form[10]

$$\langle n\alpha \mid \hat{\Sigma}(z) \mid m\beta\rangle = \sigma_\alpha(z)\delta_{nm}\delta_{\alpha\beta}. \qquad \text{(II.24)}$$

If the molecules in the unit cell are all crystallorgraphically equivalent, we can set

$$\sigma_\alpha(z) = \sigma(z) \qquad \text{(II.24')}$$

for all α. The spectral density function [Eq. (II.10)] is now given in the form

$$S(\mathbf{k}, j, E) = (\pi^{-1}) \times \frac{\mathrm{Im}\sigma(E-i0^+)}{[E-\tilde{\epsilon}-e_j(\mathbf{k})-\mathrm{Re}\sigma(E-i0^+)]^2+[\mathrm{Im}\sigma(E-i0^+)]^2}, \qquad \text{(II.25)}$$

where $e_j(\mathbf{k})$ is the energy dispersion relation in the jth exciton branch of the pure crystal. The density of states [Eq. (II.6)] can now be expressed in terms of the (complex) self-energy and the density of states $\rho^0(E)$ of the pure crystal[10]

$$\rho(E) = (N\sigma_D)^{-1}\sum_{\mathbf{k}}\sum_{j} S(\mathbf{k}, j, E) = \pi^{-1}\int dE'\rho^0(E') \times \frac{\mathrm{Im}\sigma(E-i0^+)}{[E-\tilde{\epsilon}-E'-\mathrm{Re}\sigma(E-i0^+)]^2+[\mathrm{Im}\sigma(E-i0^+)]^2} \qquad \text{(II.26)}$$

Making use of (II.9) and (II.25) the shape of the optical absorption band can be expressed in the form[10]

$$I_j(E) = \left(\frac{|\, m(j)\,|^2}{\pi}\right) \times \frac{\mathrm{Im}\sigma(E-i0^+)}{[E-\tilde{\epsilon}-t_j-\mathrm{Re}\sigma(E-i0^+)]^2+[\mathrm{Im}\sigma(E-i0^+)]^2} \qquad \text{(II.27)}$$

provided that $\mathrm{Im}\sigma$ (which determines the bandwidth) is a slowly varying function of the energy, the maximum of the absorption band is obtained from the relation

$$E-\tilde{\epsilon}-t_j-\mathrm{Re}\sigma(E-i0^+) = 0; \qquad j = 1 \cdots \sigma_D \qquad \text{(II.28)}$$

It was previously demonstrated that a pole appears in the real part of the self-energy provided that relation (II.13) is satisfied.[11] Thus in the separated band case and in the persistence case Eq. (II.28) is characterized by $2\sigma_D$ solutions, while in the amalgamation limit, Eq. (II.25) has σ_D solutions.[11]

III. THE COHERENT POTENTIAL APPROXIMATION

The CPA rests on a self-consistent approximation whereupon the effective Hamiltonian is considered as an unknown of the problem and one is seeking for the proper form of H_{eff}, determined by the restriction that a single molecule in the binary mixed crystal which scatters the electronic excitation should not produce on the average any further scattering.[11–13] The generalized perturbation resulting from the deviations of the crystal from its configurationally averaged behavior is

$$V = H - H_{\mathrm{eff}} = \sum_{n\alpha} v_{n\alpha}, \qquad \text{(III.1)}$$

where H is defined by (II.1), while H_{eff} is given by (II.4), and the local perturbation operator $v_{n\alpha}$ can be recasted by using the definition (II.2') and (II.5), and the approximate relations (II.24) and (II.24a):

$$V_{n\alpha} = (\Delta\xi_{n\alpha}+\sigma(z)) \mid n\alpha\rangle\langle n\alpha \mid . \qquad \text{(III.2)}$$

The relation between the mixed crystal Green's function $G(z) = (z-H)^{-1}$ and the configurationally averaged Green's function $\langle G(z)\rangle$ can be expressed in terms of the T matrix

$$G(z) = \langle G(z)\rangle + \langle G(z)\rangle T \langle G(z)\rangle, \qquad \text{(III.3)}$$

whereupon the exact condition for neglecting molecule–molecule spatial correlations is[11–13]

$$\langle T(z)\rangle = 0. \qquad \text{(III.4)}$$

Now invoking the assumption that multiple scattering contributions can be neglected,[10–13] Eq. (II.4) is replaced by the approximate relation

$$\langle t_{n\alpha}(z)\rangle = 0, \qquad \text{(III.4')}$$

where

$$t_{n\alpha} = (1-v_{n\alpha}(z))\langle G(z)\rangle^{-1} v_{n\alpha}(z) \qquad \text{(III.5)}$$

corresponds to a "molecular" scattering matrix associated with the site $n\alpha$. For a binary mixed crystal Eq. (III.5) is

$$C_A t_A + C_B t_B = C_A(1-v_A\langle G(z)\rangle)^{-1}v_A + C_B(1-v_B\langle G(z)\rangle)v_B = 0 \qquad \text{(III.6)}$$

where

$$V_A = (\Delta C_A - \sigma) \mid n\alpha\rangle\langle n\alpha \mid,$$

$$V_B = (-\Delta C_B - \sigma) \mid n\alpha\rangle\langle n\alpha \mid \qquad \text{(III.7)}$$

which leads to the relation

$$C_A v_A + C_B v_B = v_A\langle G\rangle v_B. \qquad \text{(III.8)}$$

The operator (II.9) can be recast in the two alternative forms[10–13]

$$\sigma(z) = (\Delta C_B - \sigma(z))f^0(z-\tilde{\epsilon}-\sigma(z))(\Delta C_A+\sigma(z)) \qquad \text{(III.9)}$$

or

$$f^0(z-\tilde{\epsilon}-\sigma(z)) = \sigma(z)/[C_A C_B \Delta^2 - \sigma(z)\Delta(C_A - C_B) + (\sigma(z))^2].$$

The auxiliary (complex) function f^0 [see also Eq. (II.7)] is defined in terms of the density of states ρ^0 of the pure crystal

$$f^0(z-\tilde{\epsilon}-\sigma(z)) = \langle n\alpha \mid \langle G \rangle \mid n\alpha \rangle = \int \{\rho^0(E')\, dE'/[z-\tilde{\epsilon}-\sigma(z)-E']\}. \quad \text{(III.10)}$$

Relations (III.10) provide us with an explicit equation for the self-energy of the mixed crystal in terms of the density of states of the pure crystal. Once $\sigma(z)$ is determined we can apply Eq. (II.26) for the density of states. Finally, utilizing the experimental information concerning the location of the Davydov components in the pure crystal, Eq. (II.27) is used for the calculations of the optical line shapes.

IV. GENERALIZATION OF THE CPA FOR A MULTICOMPONENT SYSTEM

As some experimental data for the optical spectrum of a tertiary isotopically mixed crystal were reported,[1] we shall generalize the CPA for a mixed crystal consisting of r compounds characterized by the concentrations C_i $(i=1\cdots r)$ will now be replaced by the relation

$$\sum_{i=1}^{r} C_i (1-v_i\langle G \rangle)^{-1} v_i = 0, \quad \text{(IV.1)}$$

where

$$v_i = (\eta_i - \sigma(z)) \mid n\alpha \rangle \langle n\alpha \mid . \quad \text{(IV.2)}$$

η_i is a random variable given in the form

$$\eta_i = \epsilon_i - \tilde{\epsilon}, \quad \text{(IV.3)}$$

where the mean molecular excitation energy in the crystal is

$$\tilde{\epsilon} = \sum_{i=1}^{r} C_i \epsilon_i \quad \text{(IV.3')}$$

and $\epsilon_i = \Delta\epsilon_i^I + D^I$; $\Delta\epsilon_i^I$ denoted the excitation energy of a free molecule of type i. The operator equation (IV.1) can be considerably simplified by noting that v_i is diagonal in the localized excitation representation having a single non zero matrix element $\langle n\alpha \mid v_i \mid n\alpha \rangle$. Thus the matrix equation (IV.1) can be reduced into the scalar expression

$$\sum_{i=1}^{r} C_i \langle n\alpha \mid (1-v_i\langle G \rangle)^{-1} \mid n\alpha \rangle \langle n\alpha \mid v_i \mid n\alpha \rangle = 0. \quad \text{(IV.4)}$$

The first matrix element in the sum (IV.4) is

$$\langle n\alpha \mid (1-v_i\langle G \rangle)^{-1} \mid n\alpha \rangle = [1-(\eta_i - \sigma(z))\langle n\alpha \mid \langle G \rangle \mid n\alpha \rangle]^{-1}. \quad \text{(IV.5)}$$

Equation (IV.4) now takes the form

$$\sum_i C_i \eta_i - \sigma(z)/[1-(\eta_i - \sigma(z))\langle n\alpha \mid \langle G \rangle \mid n\alpha \rangle] = 0 \quad \text{(IV.6)}$$

Finally, making use of Eq. (III.11) we get the CPA for the multicomponent system

$$\sum_i C_i [\eta_i - \sigma(z)]/[1-(\eta_i - \sigma(z)) f^0(z-\tilde{\epsilon}-\sigma(z))] = 0 \quad \text{(IV.6')}$$

Focusing attention on a three-component system (when the three components will be labeled by A, B, C), Eq. (IV.6) can be rearranged, resulting in a quadratic equation for f^0:

$$f^0(z-\tilde{\epsilon}-\sigma(z)) = [-Y \pm (Y^2-4XZ)^{1/2}]/2Z, \quad \text{(IV.7)}$$

where

$$X = \sigma(z), \quad \text{(IV.8a)}$$

$$Y = 2(\sigma(z))^2 + c\sigma(z) - a \quad \text{(IV.8b)}$$

$$Z = (\sigma(z))^3 + c(\sigma(z))^2 + (e-a)\sigma(z) - b. \quad \text{(IV.8c)}$$

The coefficients a, b, c, and e in Eq. (IV.8) are given by

$$a = c_B\Delta_1^2 + c_C\Delta_2^2 - \Delta_{12}^2, \quad \text{(IV.9a)}$$

$$b = -\Delta_{12}(\Delta_{12} - \Delta_{12}(\Delta_1+\Delta_2) + \Delta_1\Delta_2), \quad \text{(IV.9b)}$$

$$c = 3\Delta_{12} - \Delta_1 - \Delta_2, \quad \text{(IV.9c)}$$

$$e = \Delta_{12}(2\Delta_{12} - \Delta_1 - \Delta_2) + C_A\Delta_1\Delta_2, \quad \text{(IV.9d)}$$

being expressed in terms of the following energy parameters:

$$\Delta_1 = \epsilon_B - \epsilon_A, \quad \text{(IV.10a)}$$

$$\Delta_2 = \epsilon_C - \epsilon_A, \quad \text{(IV.10b)}$$

$$\Delta_{12} = C_B\Delta_1 + C_C\Delta_2. \quad \text{(IV.10c)}$$

V. A ONE DIMENSIONAL MIXED CRYSTAL

The understanding of the excited electronic states of a binary linear chain may be of some value for the elucidation of electronic states of biopolymers.[5] In the pure crystal the exciton band structure is assumed to be dominated by short range nearest neighbors interactions, so that the energy dispersion relation is just $E(k) = T\cos(ka)$, where T is the excitation transfer matrix element (or half the exciton bandwidth) and a represents the lattice spacing. The pure crystal density of states is

$$\rho^0(E) = \pi^{-1}(T^2-E^2)^{-1/2}. \quad \text{(V.1)}$$

Utilizing Eq. (V.1), we find for the configurationally averaged Green's function in the localized representation [Eq. (III.11)]

$$f^0(x) = i/(T^2-x^2)^{1/2}, \quad \text{(V.2)}$$

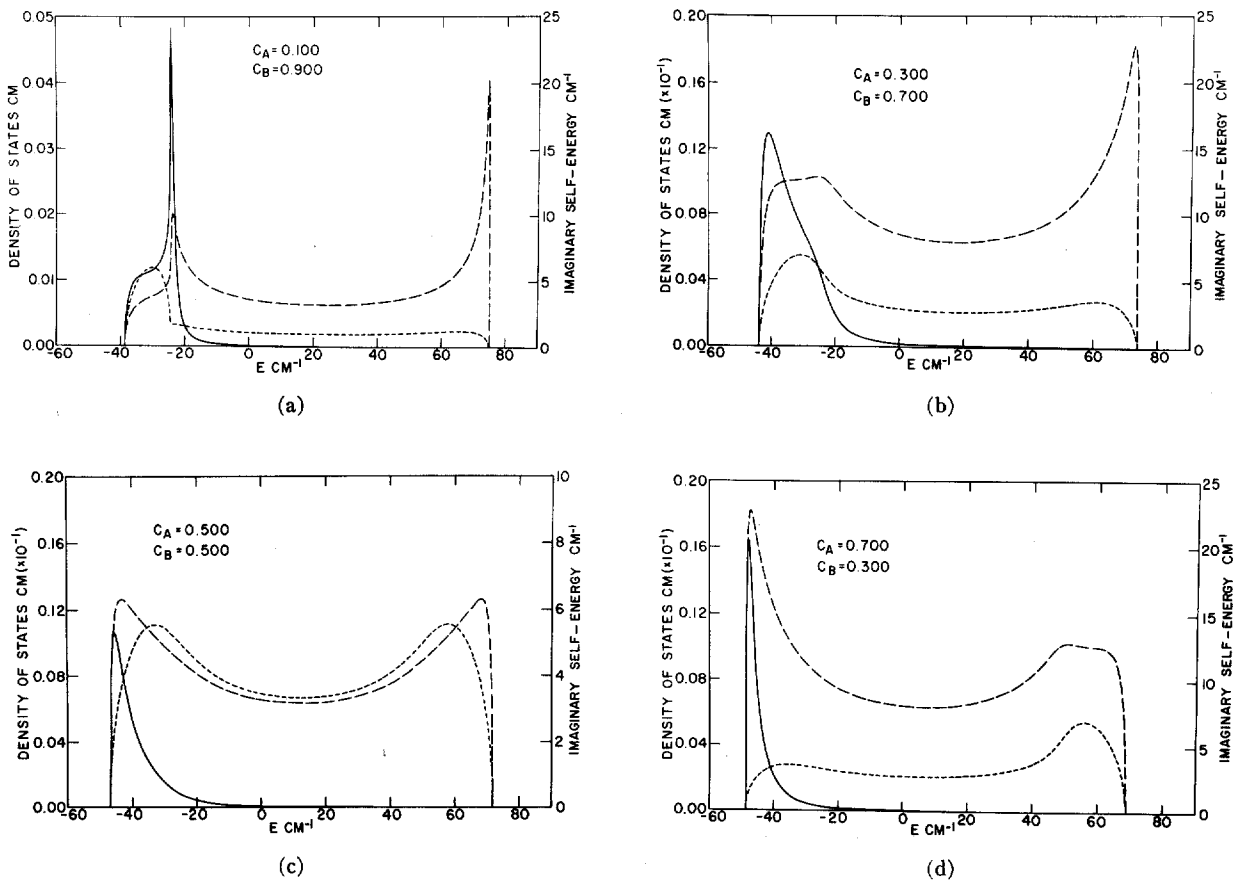

FIG. 1. Level distribution and optical properties of a one dimensional crystal. $T=50$ cm^{-1}, $\Delta=25$ cm^{-1}. - - -, imaginary self-energy; – –, density of states; —, optical line shapes.

where the complex variable x is

$$x=z-\tilde{\epsilon}-\sigma(z)=z-(\Delta\epsilon_A{}^f+D^f)-C_B\Delta-\sigma(z). \quad \text{(V.3)}$$

It will be convenient to shift the real part of the origin of z setting $x=z-C_B\Delta-\sigma(z)$. Now, combining Eqs. (V.2) and (V.3) with (II.10) results in a cubic equation for the self-energy of a mixed one dimensional chain

$$[\sigma(z)]^3(C_B\Delta-z)+[\sigma(z)]^2(z^2-2zC_A\Delta-C_B{}^2\Delta^2 +4C_AC_B\Delta^2-T^2)+2[\sigma(z)]C_AC_B(C_A-C_B)\Delta^3 -C_A{}^2C_B{}^2\Delta^4=0. \quad \text{(V.4)}$$

In the energy range where the density of states is nonvanishing the self-energy is complex. We shall therefore search for z values where the solutions of the cubic Eq. (V.4) yield two roots which are complex conjugate. The third real root is regarded to be unphysical and will be consequently disregarded. Finally, Eqs. (II.26) and (II.27) were applied for the calculation of the density of states of the optical line shape.

As a first numerical example we now specialize to the one dimensional mixed crystal specified by the following parameters: $T=50$ cm^{-1}, $\mu_2{}^0=T^2/2=1250$ cm^{-1}, and where the optical absorption band in the pure crystal is located at the bottom of the band ($t=-50$ cm^{-1}). Numerical calculations were performed over a wide range of Δ and C values. In Figs. 1–3 we display the imaginary part of the self-energy, the density of states, and the optical line shapes in the concentration region $C_A=0.1$–0.9 for several Δ values ranging from the amalgamation limit up to the separated bands case. In order to get some feeling for the conditions which determine the appearance of the a bandgap in the density of states of this mixed model system, we have investigated the discriminant of the cubic Eq. (V.4) determining the values of Δ and C where this equation has only real solutions in the relevant energy region. Consequently we were able to specify in Fig. 4 the following regimes:

(a) The amalgamation region which corresponds to low values of Δ and to finite C_A and C_B concentrations. Here both the imaginary part and the real parts of the self-energy vary slowly over the whole energy range resulting in a single band.

(b) Above the amalgamation region the imaginary part of the self-energy and the density of states reveal a

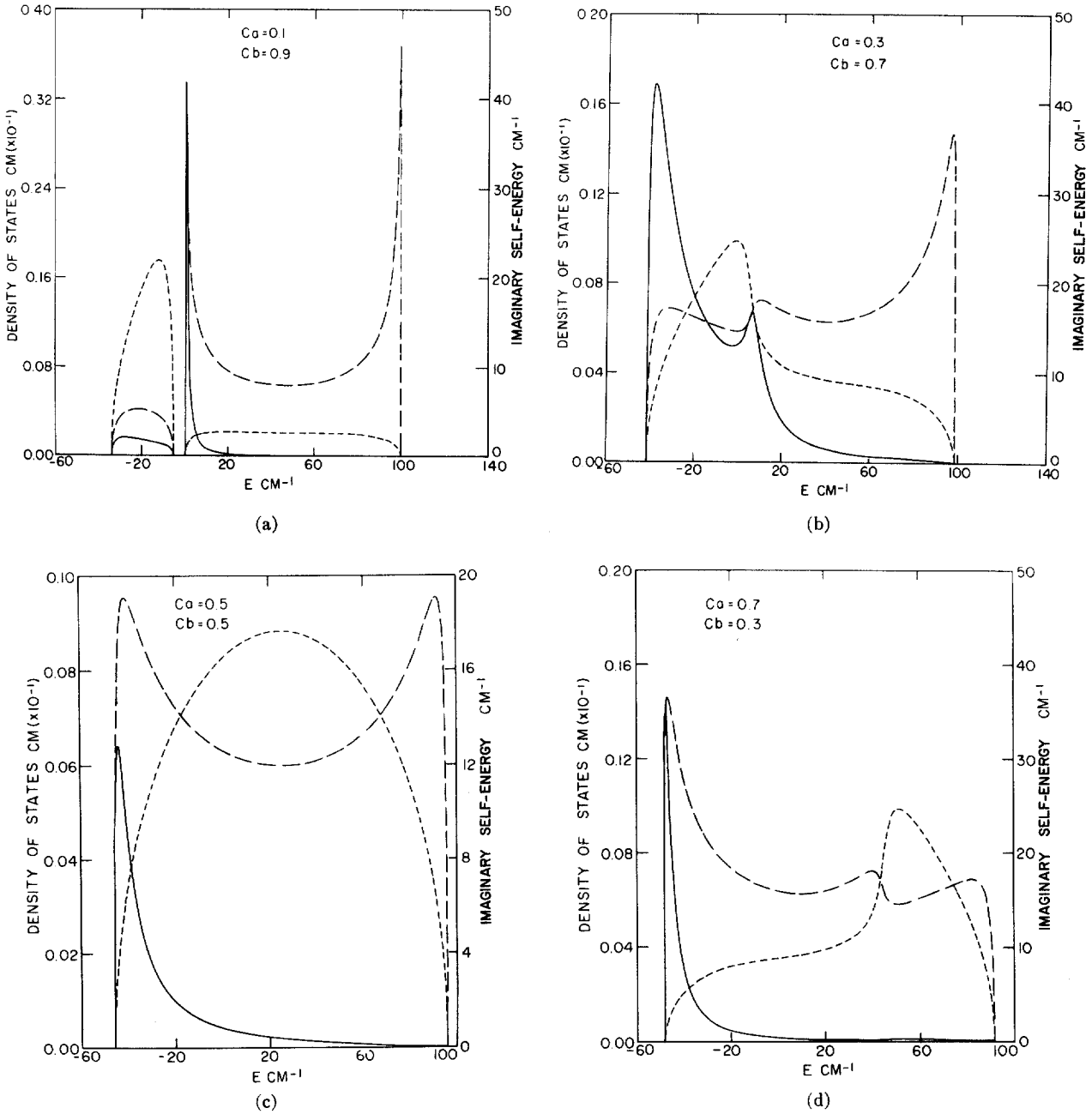

FIG. 2. Level distribution and optical properties of a one dimensional crystal. $T=50$ cm^{-1}, $\Delta=50$ cm^{-1}. Notation identical to that of Fig. 1.

gap. In the limit $C_A \to 0$ or $C_B \to 0$ the minority and majority bands split for an arbitrary weak perturbation strength (any finite Δ). This result is not surprising as in the low concentration limit, the CPA reduces properly to the exact result for a single impurity, and it is well known that for a one dimensional crystal a single local perturbation will always split a state outside the band.[5] At finite concentrations the critical Δ value required to produce the band gap increases, reaching the value $\Delta=T/\sqrt{2}$ at $C_A=C_B=0.5$. These results based on the CPA are consistent with the necessary condition (II.12) for the persistence case, and it should be noted that splitting of the bands occurs for somewhat weaker perturbation strength $(C_A C_B \Delta^2)^{1/2}$ than specified by (II.12).

(c) In the region above the dashed upper line in Fig. 4 the real part of the self-energy exhibits a pole. The condition for the appearance of this pole within the framework of the CPA is identical to the general condition (II.12). In our case the lowest value of Δ for

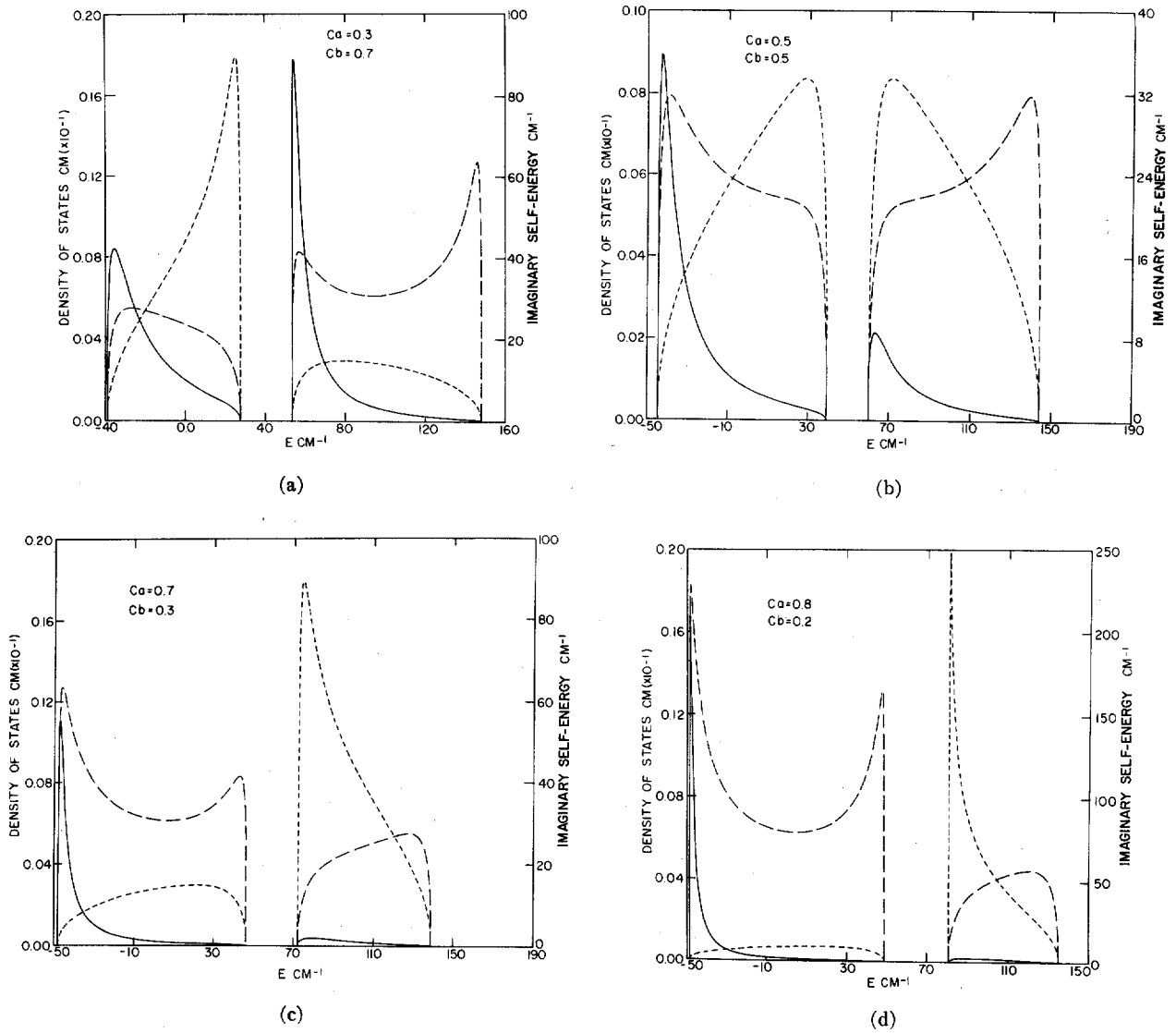

FIG. 3. Level distribution and optical properties of a one dimensional crystal. $T=50$ cm^{-1}, $\Delta=100$ cm^{-1}. Notation identical to that of Fig. 1.

which a pole is observed is given by $C_A(1-C_A)\Delta^2=1250$ cm^{-2}. The region above this dashed line obviously exhibits the persistence case.

Consider now some of the features of the absolute value of the imaginary part of the self-energy (Figs. 1–3):

(a) In the amalgamation case [Fig. 1 and Figs. 2(b)–2(d)] the zeroth moment of the self-energy obeys the general sum rule[11]:

$$\int_{-\infty}^{\infty} dE\ \mathrm{Im}\sigma(E-io^{\dagger})=\pi C_A C_B \Delta^2, \qquad \text{(V.5)}$$

whereupon disorder scattering is most efficient for equal concentrations of the two components.

(b) In the persistence case and in the separated band limit the contributions of the self-energy to the two subbands are given by the approximate sum rules[11]:

$$\int_{\alpha\ \text{band}} dE\ \mathrm{Im}\sigma(E-io^{\dagger})=\pi C_B \mu_2{}^0;$$

$$\int_{\beta\ \text{band}} dE\ \mathrm{Im}\sigma(E-io^{\dagger})=\pi C_A \mu_2{}^0 \qquad \text{(V.6)}$$

so that the ratios of the zeroth moments of the self-energy are C_B/C_A. It should be noted that Eq. (V.6) is approximate, being valid for large values of Δ/T. From the data in Fig. 3 ($\Delta/T=2$) we assert that indeed the contribution of the self-energy in the minority band is larger than in the majority band and that the ratio of the corresponding areas is given by C_B/C_A.

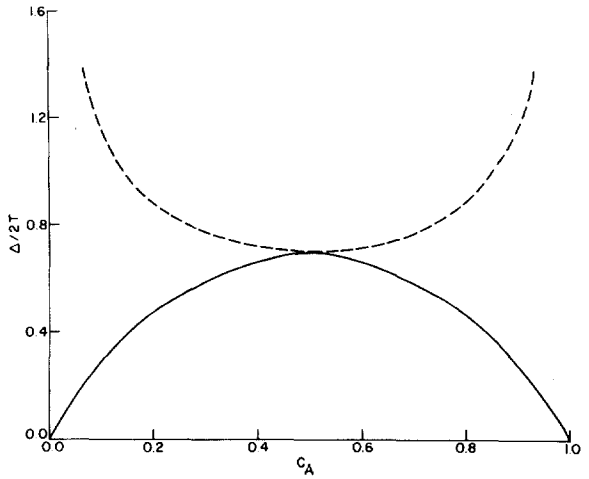

FIG. 4. Regions of amalgamation and persistence limits in the CPA, for a one dimensional crystal. The lower region corresponds to the amalgamation limit and above the solid curve the bands are split. The upper dashed line represents the onset of a pole in the real part of the self energy.

Turning our attention now to density of states (Figs. 1–3) obtained by the CPA we notice the following:

(a) The calculated densities of states are symmetric in the concentrations of the two components, in accordance with the general features of the CPA.

(b) The Van Hove singularities in the density of states of the pure crystal are erased due to disorder scattering.

(c) In the amalgamation case (Fig. 1) the second moments of the density of states are given by Eq. (II.17) so that the "width" of the distribution of states is given by $[\mu_2^0-\frac{1}{2}\Delta(C_A-C_B)^2+\Delta^2/4]^{1/2}$. The data in Fig. 1 confirm this expectation.

(d) In the persistence case close to the separated bands limit (Fig. 3) the moments of the density of states are given by Eq. (II.16b). Finally, let us consider the features of the optical line shapes:

(a) Unlike the density of states the intensity distribution in absorption for this model crystal which contains one molecule per unit cell is not symmetrical in the two components. This result can be immediately rationalized by the fact that the line shape is always determined by the spectral density function at $\mathbf{k}=0$.

(b) In the amalgamation limit (Fig. 1) all the intensity in the optical spectrum of the mixed crystal is centered near the bottom of the band, exhibiting broadening of the pure crystal band by impurity scattering. The "width" of the spectral distribution confirms Eq. (II.23). When the perturbation is increased [see Fig. 2(b)], rather peculiar line shapes result exhibiting a double hump. Nevertheless, the moments still follow general relation (II.23). In Fig. 5 we have displayed the result of numerical calculations of the total widths of the spectral distributors for $T/\Delta=1$. As expected, Eq. (II.23) is fulfilled.

(c) Finally, when a bandgap is formed in the density of states, two intensity distributions in the absorption spectrum are exhibited near the lower edges of the two subbands (see Fig. 4). The centers of gravity and the widths of the intensity distributors are quite well reproduced by Eqs. (II.19) and (II.20).

It is interesting to obtain some rough idea concerning the "band structure" of the disordered system. In an ordered system the band structure has, of course, a precise and well defined meaning, being described in terms of the dependence of the energy in the crystal quasimomentum. Alternatively, one may state that in the pure crystal the spectral density [Eq. (II.10)] takes the form of a delta function, so that to each energy eigenstate there corresponds a single $\mathbf{k}$ vector. In the disordered system, the quasimomentum is not a good quantum number. The spectral density (II.25) has now a finite width, as in view of disorder scattering, any energy state corresponds to a whole distribution of $\mathbf{k}$ vectors. $S(\mathbf{k}, j, E)$ can be considered as a function of E for any fixed k, so that the half-width specifies the spread of the energy eigenstates corresponding to that k vector. In Figs. 6(a) and 7(a) we display the spectral density function for the amalgamation and for the persistence cases. In Figs. 6(b) and 7(b) we present the approximated description of the energy dispersion curves in the disordered system. The solid line represents the maxima of the spectral density functions while the dashed curves represent the corresponding energy values (at each $\mathbf{k}$) where the spectral density has dropped to half of the value obtained at the peak. Thus in the amalgamation limit one broadened band results, while in the persistence case two broadened bands are obtained. It should also be noted that the broadening of the states in the middle of the band is much larger than at the band edges. At the band extremes the ratio of the broadening to the bandwidth

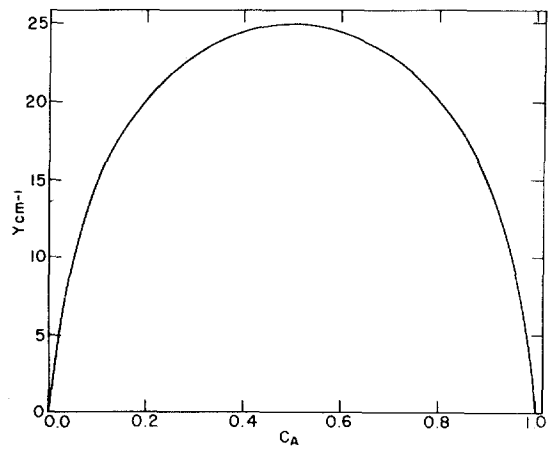

FIG. 5. The width Y of the intensity distribution for a on dimensional crystal, calculated by the CPA. $T=\Delta=50$ cm^{-1}.

is about 0.1 and **k** is a "fairly good" quantum number. In the middle of the "energy band" the ratio of the broadening to the total energy bandwidth is about 0.5, exhibiting a very serious departure from the pure **k** exciton states.

To conclude this discussion of the features of the one dimensional model system, we should point out that the configurational averaging procedure which provides the ideological basis for the CP approximation may be rather poor for a one dimensional system. As the local environment of each atom in this case consists of a small number of neighboring molecules, the role of molecule-molecule spatial correlation will be of considerable importance.

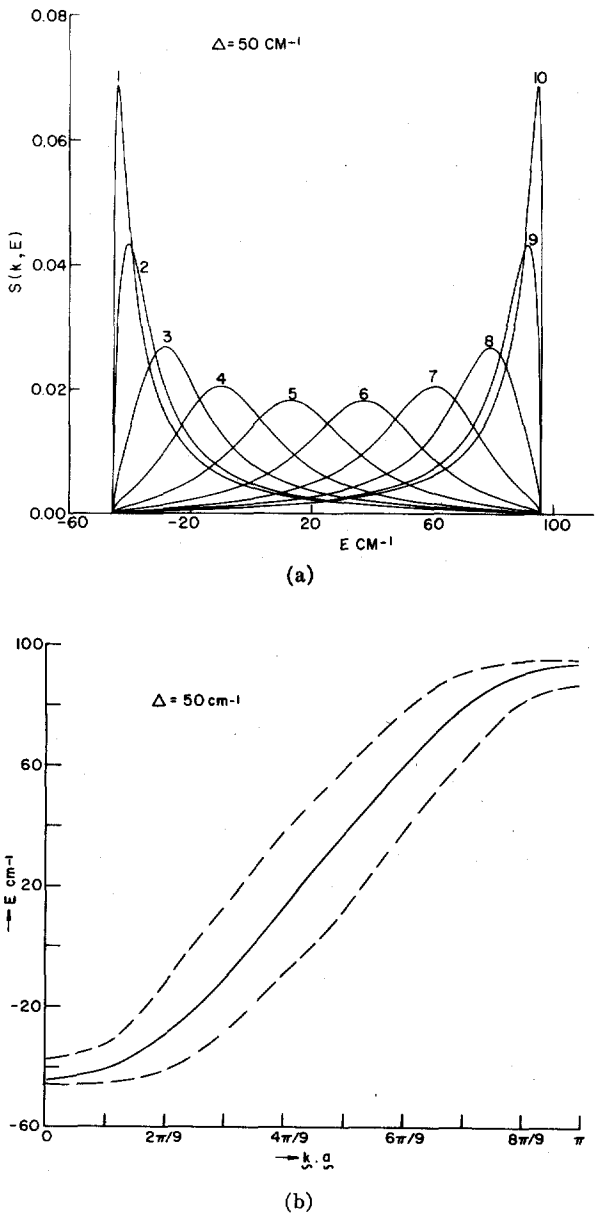

FIG. 6. Spectral density functions and rough energy dispersion curves for a one dimensional model system in the amalgamation limit. $T=50$ cm^{-1}; $\Delta=50$ cm^{-1}; $C_A=C_B=0.5$. (a) Spectral density functions. The numbers $n=1\cdots10$ represent the values of $k=(n-1)\pi/9a$. (b) The k dependence of the maxima and half-width of the spectral density functions providing a rough description of the "band structure" of the disordered system.

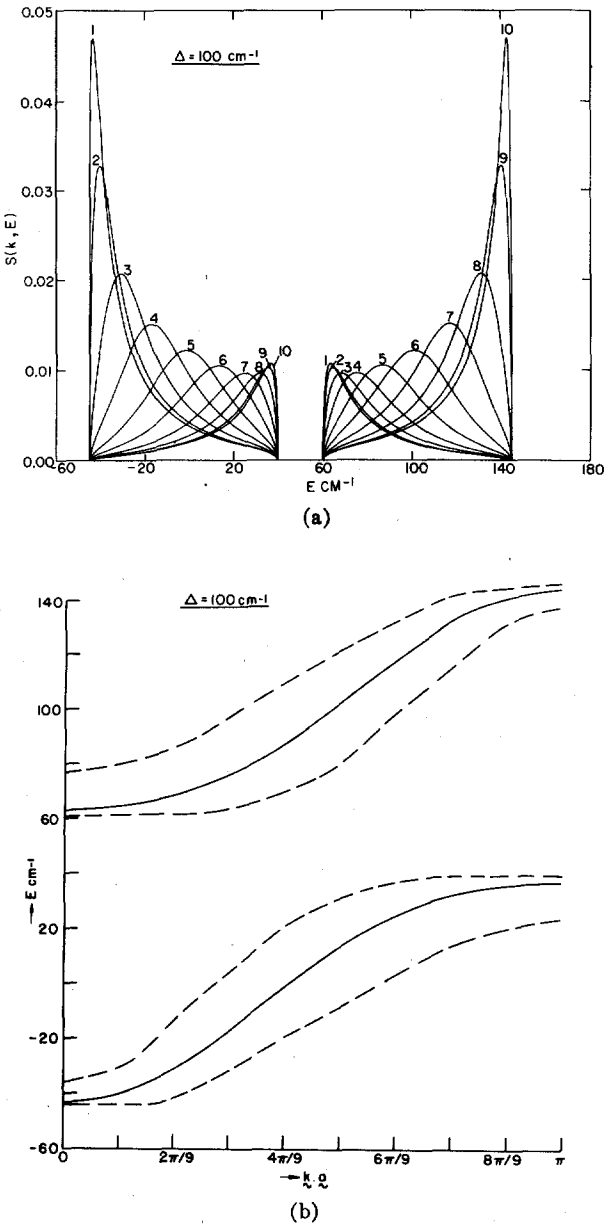

FIG. 7. Spectral density functions and rough energy dispersion curves for a one dimensional system in the persistence case. $T=50$ cm^{-1}; $\Delta=100$ cm^{-1}; $C_A=C_B=0.5$. (a) Spectral density functions, the numbers $n=1\cdots10$ representing the values of $k=(n-1)\pi/9a$. (b) The k dependence of the maxima and of the half-width of the spectral density functions.

VI. TRIPLET STATES IN SUBSTITUTIONALLY MIXED CRYSTALLINE NAPHTHALENE

The exciton band structure corresponding to the lowest triplet state (molecular parentage $^3B_{2u}$) in pure

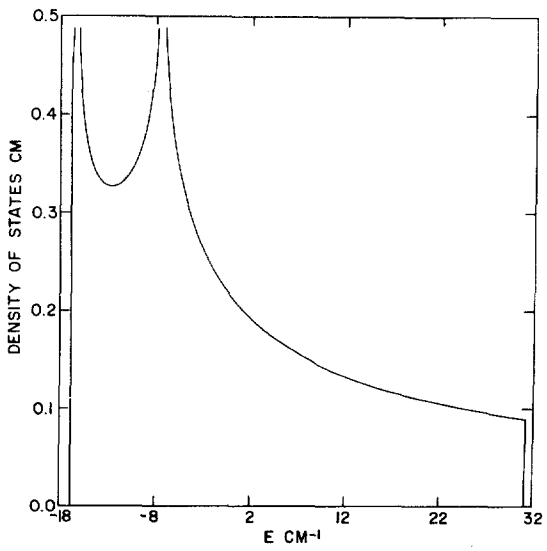

FIG. 8. Triplet exciton band structure in crystalline naphthalene calculated from the analytic expression (VI.2)–(VI.4).

crystalline naphthalene (a monoclinic crystal containing two molecules per unit cell) has been extensively studied both theoretically and experimentally.[15,16] The pure crystal exciton energy dispersion curve is determined by short range interactions in the ab crystal plane, the two exciton branches being given by[15b]

$$e_{1,2}(\mathbf{k}) = p\cos(\mathbf{k}\cdot\mathbf{b}) \pm 2q\cos[\tfrac{1}{2}(\mathbf{k}\cdot\mathbf{b})]\cos[\tfrac{1}{2}(\mathbf{k}\cdot\mathbf{a})], \tag{VI.1}$$

where $p=2\epsilon(b)$ and $q=2\epsilon[\frac{1}{2}(a+b)]$. Here $\epsilon(b)$ represents the exchange excitation transfer integral between the nearest adjacent translationally equivalent molecules located on the monoclinic b axes, while $\epsilon[\frac{1}{2}(a+b)]$ corresponds to the interaction term between translationally unequivalent molecules in the ab plane. The density of states in the triplet band was previously obtained by numerical methods.[15b] Alternatively, the density of electronic states $\tilde{\rho}^0(E)$ for the system can be represented in a closed form in terms of a complete elliptic integral of the first kind[17]:

$$\tilde{\rho}^0(E) = gK(\kappa'), \tag{VI.2}$$

where K is a complete integral of the first kind. κ' is the complementary modulus, $\kappa'=(1-\kappa^2)^{1/2}$, and

$$\kappa = \frac{2q^2+p^2-E^2-2\,|\,q\,|\,(2p^2+2Ep+q^2)^{1/2}}{2q^2+p^2-E^2+2\,|\,q\,|\,(2p^2+2Ep+q^2)^{1/2}}; \tag{VI.3}$$

the coefficient g in (VI.2) is

$$g=2\{\pi^2[2q^2+pE-E^2+2q(2p^2+2Ep+q^2)^{1/2}]^{1/2}\}^{-1}. \tag{VI.4}$$

The resulting pure crystal density of states calculated from (VI.2)–(VI.4) using[15] $p=7.4$ cm^{-1} and $q=-11.8$ cm^{-1} is displayed in Fig. 8 and is in good agreement with previous numerical calculations. Now, this triplet exciton state in the pure crystal corresponds to the weak electronic–vibrational coupling, so that the total electronic contributions to the dispersion curve (VI.1) and to the density of states (VI.2) have to be partitioned between various $0\rightarrow V$ ($V=0,\ 1\cdots$) vibronic transition by the Franck–Condon vibrational overlap integrals FC(V). Thus the effective interaction terms in (VI.1) are $p\mathrm{FC}(V)$ and $q\mathrm{FC}(V)$, while the density of state in a given vibronic band, $\rho^0(E)$, is scaled to give $\rho^0(E)=[\mathrm{FC}(V)]^{-1}\tilde{\rho}^0(E/\mathrm{FC}(V))$. We have chosen the Franck–Condon factors from the available experimental data[16] $\mathrm{FC}(0)=0.208$, $\mathrm{FC}(1)=0.166$, and $\mathrm{FC}(2)=0.125$ to yield pure crystal vibronic densities of states characterized by the total widths $W=10$ cm^{-1} for the $0\rightarrow 0$ vibronic component $W=8$ cm^{-1} for the $0\rightarrow 1$ vibronic component and $W=6$ cm^{-1} for the $0\rightarrow 2$ vibronic component.[16] This information is sufficient for the calculation of the density of states in the isotopically mixed crystal. For the calculation of the optical line shapes the position of the Davydov components in the pure crystal were taken to be $t_1=(p+2q)\ \mathrm{FC}(V)$ and $t_2=(p-2q)\ \mathrm{FC}(V)$.

Numerical calculations by the CPA were performed for the lowest triplet exciton state in isotopically mixed α-$C_{10}H_7D/C_{10}H_8$ crystals. The perturbation strength was taken to be identical to that for the lowest singlet excited state of naphthalene $\Delta=14$ cm^{-1}. This perturbation strength was kept constant while the pure crystal bandwidth was varied in the range $W=10$–6 cm^{-1}. As $\Delta W>1$, this physical situation corresponds to the separated bands limit. Thus a gap will appear in the imaginary part of the self-energy and in the density of states, the real part of the self-energy will exhibit a pole, and four intensity distributions (two in the range of each subband) will be revealed in the optical spectrum. For the two dimensional system discussed herein and for three dimensional systems (see Sec. VII), numerical methods have to be applied. The details of the numerical calculations are summarized in the Appendix. It should be noted that we were able to overcome some computational problems such as convergence and spurious oscillators of the density of states near the band edges.

In Fig. 9 we display typical CPA results for the self-energy, the density of states, and the optical line shapes for the lowest vibronic triplet state of an isotopically mixed naphthalene crystal. The lower moments of the density of states in the two separated subbands are reasonably well described in terms of Eq. (II.17b). The concentration dependence of the density of states exhibits nicely the erosion of the Van Hove singularities due to disorder scattering. While at low concentrations the majority subband still reveals a behavior which is reminiscent of the logarithmic singularities within the band, these singularities disappear

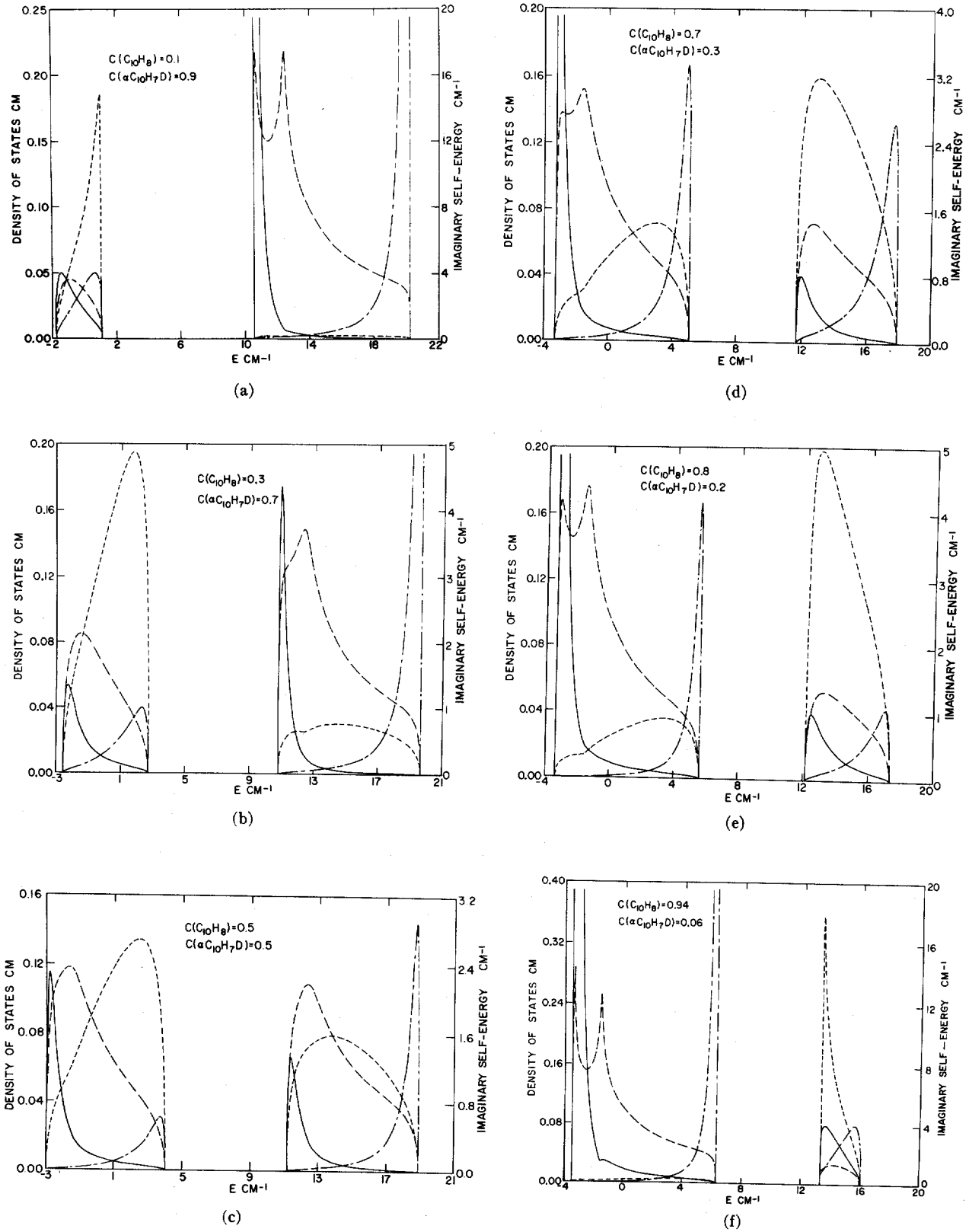

FIG. 9. Level distribution and optical properties of the lowest triplet state in isotopically mixed crystalline naphthalene. $W=10$ cm^{-1}, $\Delta=14$ cm^{-1}. - - -, imaginary self-energy; – –, density of states; —, b polarized absorption band; — - — -, ac polarized absorption band.

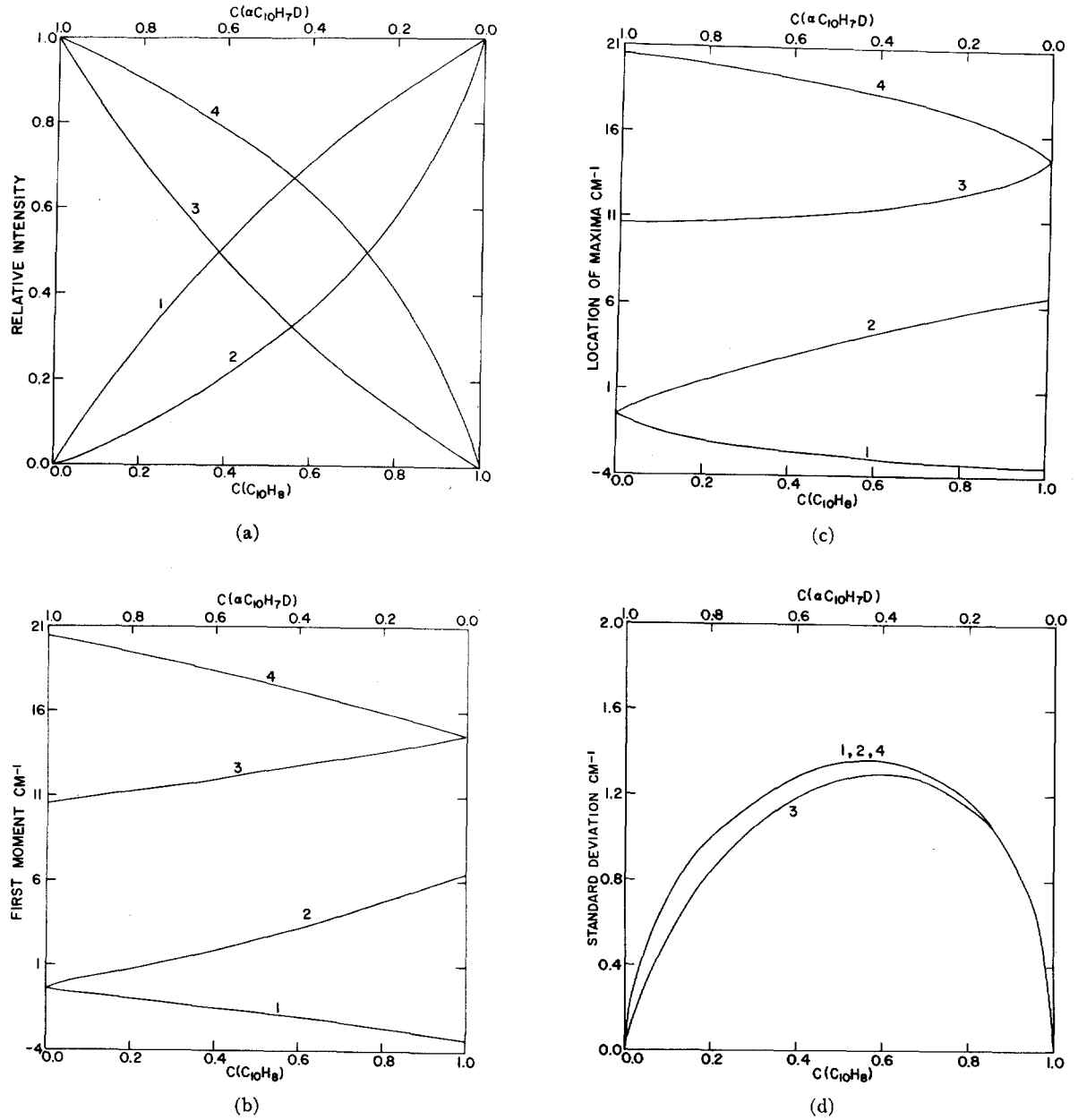

FIG. 10. Optical properties of the 0–0 vibronic component of the lowest triplet state in $C_{10}H_8/\alpha$-$C_{10}H_7D$ mixtures. $W=10$ cm^{-1}; $\Delta=14$ cm^{-1}. 1, lowest b polarized transition; 2, lowest ac polarized transition; 3, higher b polarized transition; 4, higher ac polarized transition. (a) Relative intensities. (b) First moments of absorption bands. (c) Location of maxima of absorption bands. (d) Half bandwidths.

in the heavily doped crystal. The physical situation discussed herein corresponds to the separated bands situation. We should note in passing that any arbitrarily weak perturbation strength (such as ^{13}C substitution which is equivalent to $\Delta\sim3$ cm^{-1}) in this system will result in separated bands in the low concentration limit C_B, $C_A\to0$, exhibiting a basic feature of the two dimensional system.

Turning our attention now to the optical properties, four polarized optical absorption bands are expected to be observed in the separated bands limit. We have displayed in Fig. 10 the following properties of these optical absorption bands: (a) The total intensity (zeroth moments); (b) the band maxima; (c) the first moments; (d) the band half-widths (obtained from the first and from the second moment). In view of the deviations of the optical line shapes from a Lorentzian, there is a marked difference between the location of the band maximum and of the first moment. The concentration dependence of the band maxima is parabolic, while the first moment exhibits a concentration dependence which is close to linear. The most easily

observable physical property involves the Davydov splittings in the two subbands. These theoretical data for the band maxima are summarized in Fig. 11. It is worthwhile noting that the gross features of the concentration dependence of the zeroth moment, the first moment, and the bandwidth obtained by the CPA are in qualitative agreement with the prediction of the general moment expansion method [Eqs. (II.18)–(II.20)].

Finally, it is of some interest to obtain a rough description of the "band structure" of the two dimentional disordered system. Following the discussion presented in Sec. V for the one dimensional system, we display in Figs. 12(a) and 13(a) the spectral density functions $S(\mathbf{k}, j, E)$ for the two excitation branches ($j=1, 2$) calculated from (II.25), and (VI.1) for the triplet state in isotopically mixed naphthalene. The maxima and the half-widths of $S(\mathbf{k}, j, E)$ [see Figs. 12(b) and 13(b)] provide us with a rough idea concerning the smearing of the pure ideal crystal band structure due to impurity scattering. Again, as in the one dimensional case the broadening of the states in the middle of the "energy band" is considerably larger than at the "energy band" edges.

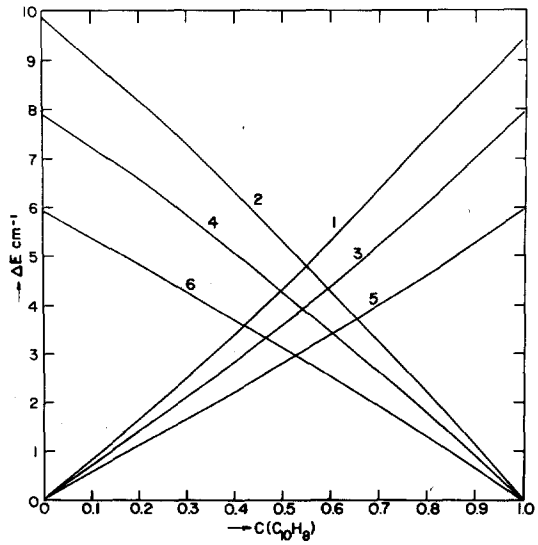

FIG. 11. Davydov splittings for various vibronic components in the first triplet state of $C_{10}H_8/\alpha$-$C_{10}H_7D$ mixed crystals. 1, 2: $W=10$ cm^{-1}; 3, 4: $W=8$ cm^{-1}; 5, 6: $W=6$ cm^{-1}.

VII. THE LOWEST EXCITED SINGLET STATE OF HEAVILY DOPED CRYSTALLINE NAPHTHALENE

Experimental studies[1–3] of the lowest singlet excited state in isotopically mixed napthalene crystals provided the impetus for the theoretical activity in this field. In his pioneering experimental work, Sheka has demonstrated the persistence of the Davydov components (in fact, three polarized bands were observed) in $C_{10}H_8/C_{10}D_8$ and in $C_{10}H_8/\beta$-$C_{10}H_4D_4$ mixed crystals. These systems correspond to the persistence case.[7–10] Recently, Hong and Robinson[9] extended these experi-

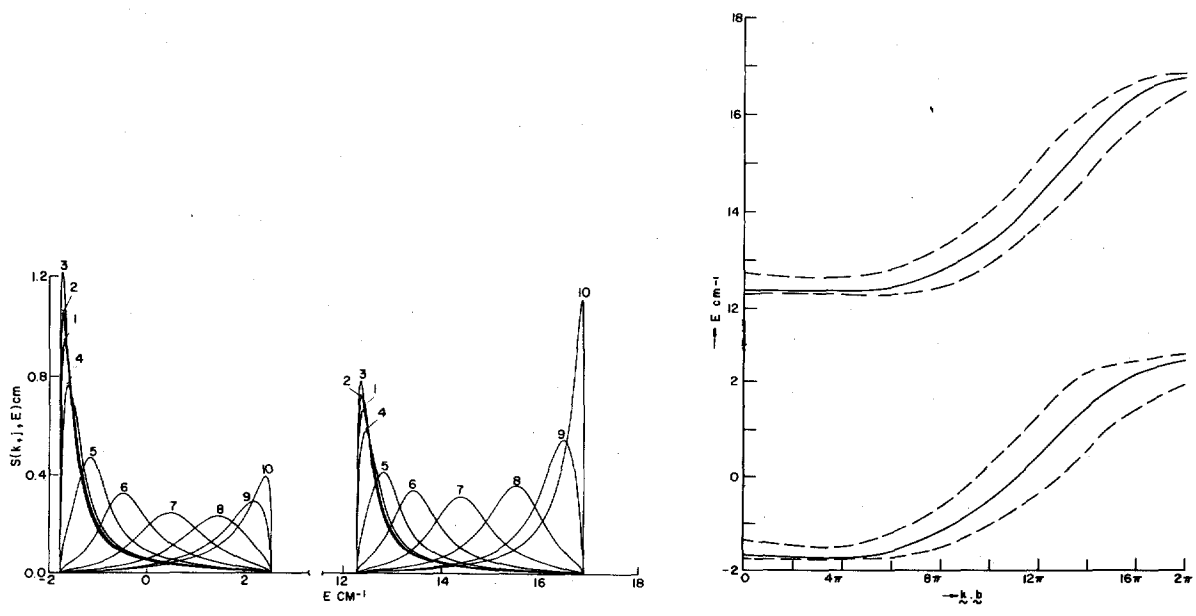

FIG. 12. Spectral density functions and rough energy dispersion curves in the **b** crystal direction for triplet states in mixed naphthalene crystals. $\Delta=14$ cm^{-1}, $W=10$ cm^{-1}, $C_A=C_B=0.5$. (a) Spectral density functions ($j=1$). The numbers $n=1\cdots10$ refer to the values $\mathbf{k}\cdot\mathbf{b}=2(n-1)\pi/9$. (b) The k dependence of the maxima and of the half-width of the spectral density functions in the **b** direction.

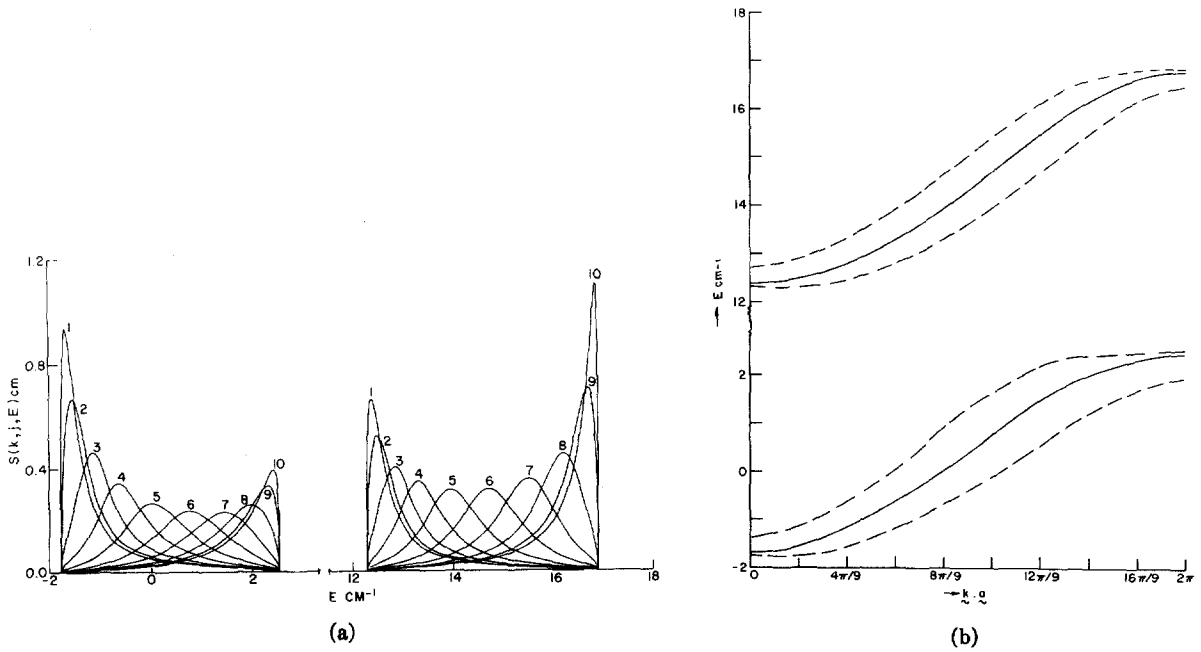

FIG. 13. Spectral density functions and rough energy dispersion curves in the a crystal direction for triplet states in mixed naphthalene crystals $\Delta=14$ cm^{-1}; $W=10$ cm^{-1}; $C_A=C_B=0.5$. (a) Spectral density function ($j=2$). The numbers $n=1\cdots10$ refer to the value of $\mathbf{k}\cdot\mathbf{a}=2(n-1)\pi/9$. (b) The $\mathbf{k}$ dependence of the maxima and of the half-width of the spectral density functions in the $\mathbf{a}$ directions.

mental studies recording the spectra of $C_{10}H_8/C_{10}D_8$ (the persistence case), $C_{10}H_8/\alpha$-$C_{10}H_4D_4$ (the amalgamation limit) and $C_{10}H_8/\alpha$-$C_{10}H_7D$ (the amalgamation limit). The first theoretical scheme for the electronic states of these mixed crystals was proposed by Broude and Rashba[2] invoking the hypothesis of "exciton democracy," that is, the amplitudes of the local excitations are determined by the site occupation and by the molecular orientation in the unit cell. Hong and Robinson[7,9] and the present authors[8] have applied the Onodera–Toyozawa[6] scheme (which is equivalent to the CPA for a crystal characterized by one molecule per unit cell) to this system. Finally a systematic study of the CPA for a multibranched exciton band was provided by us.[10] Hong and Robinson have presented a detailed comparison between their experimental results[9] and the theoretical treatment[7,8] based on the Onodera–Toyozawa scheme and on the Broude–Rashba[2] formalism. They conclude that the difference between the two schemes involves different starting points and that the Broude–Rashba[3] scheme does not take the random distribution of impurities into account. We would like to point out that the Broude–Rashba[3] scheme does properly account for configurational averaging. As was recently demonstrated by us the Broude–Rashba equation can be derived from the CPA in the atomic limit,[10] i.e., when $\mu_2^0\to0$. It is thus not surprising that the Broude–Rashba[3] scheme yields the persistence limit for any arbitrarily weak perturbation strength, and for most cases of physical interest this scheme is not applicable.

As the binary naphthalene mixed crystals have been previously extensively studied[7–10] we shall present only a brief survey of our theoretical results based on the CPA, which are complementary to the theoretical work of Hong and Robinson.[9] The input data pertaining to the properties of the crystal are: (a) the density of states obtained from hot band spectroscopy,[18] which is characterized by the second moment $\mu_2^0=1410$ cm^{-2}; (b) the positions of the Davydov components $t_1=+78$ cm^{-1} and $t_2=-78$ cm^{-1}; (c) the perturbation strengths[4,19,20] $\Delta=115$ cm^{-1} for $C_{10}H_8/C_{10}D_8$, $\Delta=74$ cm^{-1} for $C_{10}H_8/\beta$-$C_{10}H_4D_4$, $\Delta=51$ cm^{-1} for $C_{10}H_8/\alpha$-$C_{10}H_4D_4$, $\Delta=26$ cm^{-1} for $C_{10}H_8/\beta$-$C_{10}H_7D$, and $\Delta=14$ cm^{-1} for $C_{10}H_8/\alpha$-$C_{10}H_7D$. The details of the numerical calculations are given in the Appendix.

In Fig. 14 we summarize the regimes of the coherent potential approximation for binary mixed naphthalene crystals. In the lower region below the solid curve, the amalgamation limit is encountered; a single band is observed in the imaginary part of the self-energy and consequently in the density of states, while the real part of the self-energy is a slowly varying function of the energy throughout the band. In the vicinity of the solid curve, an incipient bandgap results and above it the bands are split, representing the onset of the persistence case. It should be noted that unlike the one dimensional (Fig. 4) and the two dimensional systems in the limit of low concentrations, the bands are split only for a finite perturbation strength. It is also worthwhile noting that as the density of states function is asymmetric the separation between the CPA amalga-

mation and the CPA persistence case results in an asymmetric curve. The upper dashed curve in Fig. 14 corresponds to the onset of a pole in the real part of the self-energy, being determined by the relation $C_A(1-C_A)\Delta^2=1410$ cm^{-2}. Above this curve four Davydov components will always be observed in the optical spectrum. We have performed detailed calculations of the self-energy, the density of states, and the optical line shapes for several types of binary naphthalene crystals. The zeroth moment of Imσ in the amalgamation limit ($C_{10}H_8/\alpha$-$C_{10}H_7D$, $C_{10}H_8/\beta$-$C_{10}H_7D$, and $C_{10}H_8/\alpha$-$C_{10}H_4D_4$) fulfills the relation (V.5), while in the persistence case ($C_{10}H_8/C_{10}D_8$) the contributions of the imaginary self-energy to the two subbands confirms Eq. (V.6). The moments of the density of states in the amalgamation limit ($C_{10}H_8/\alpha$-$C_{10}H_7D$, $C_{10}H_8/\beta$-$C_{10}H_7D$, and $C_{10}H_8/\alpha$-$C_{10}H_4D_4$) are well given by (II.16a), while in the persistence case ($C_{10}H_8/\beta$-$C_{10}H_4D_4$ and $C_8H_8/C_{10}D_8$) the relative contributions of the subbands are well reproduced by the approximate relation (II.16b).

In the discussion of the optical properties we would again like to stress the point that the number of Davydov components observed in the mixed crystal is determined by the behavior of the real part of the self-energy.[10] In Fig. 15 we have displayed the values of Reσ for several perturbation strengths and several concentrations. In the amalgamation limit [Figs. 15(a) and 15(b)] the real part of the self-energy varies slowly over the (single) band region, and consequently Eq. (II.28) yields two solutions, corresponding to two intensity distributions. In the persistence case [Fig. 15(c)] a pole is observed in Reσ so that Eq. (II.28) now results in four polarized intensity distributions.

In Figs. 16–19 we display the CPA results for the

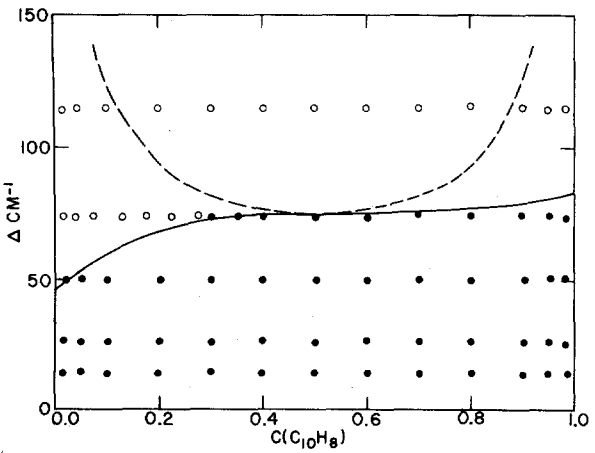

FIG. 14. Regions of the CPA for binary mixed naphthalene crystals. The lower solid curve represents the onset of the bandgap in the density of states. The dashed curve corresponds to the onset of a pole in the real part of the self-energy. The points indicate the values of C and Δ at which numerical computations were performed (closed circles represent amalgamation, for the open circles the bands are split).

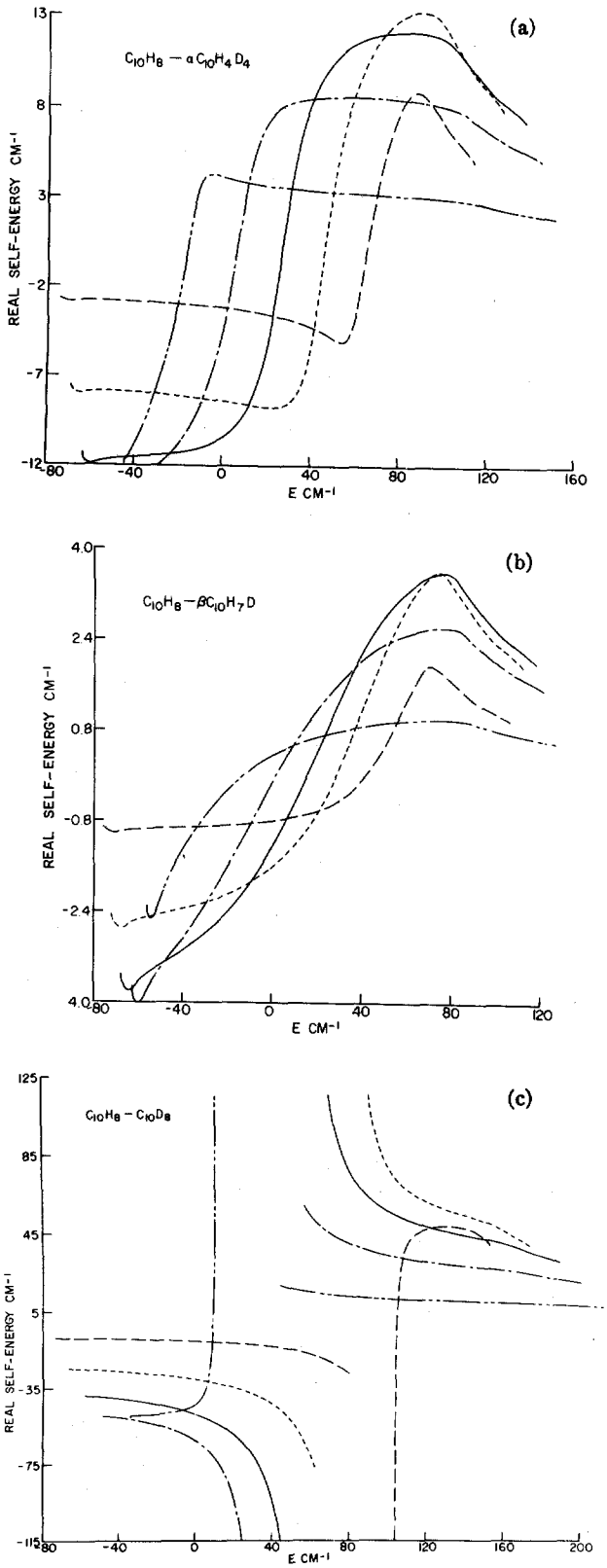

FIG. 15. The real part of the self-energy in mixed naphthalene crystals. —, $C_A=0.5$; – – –, $C_A=0.7$; - - -, $C_A=0.3$; - - - -, $C_A=0.9$; – – –, $C_A=0.1$. (a) $\Delta=14$ cm^{-1}; (b) $\Delta=26$ cm^{-1}; (c) $\Delta=114$ cm^{-1}.

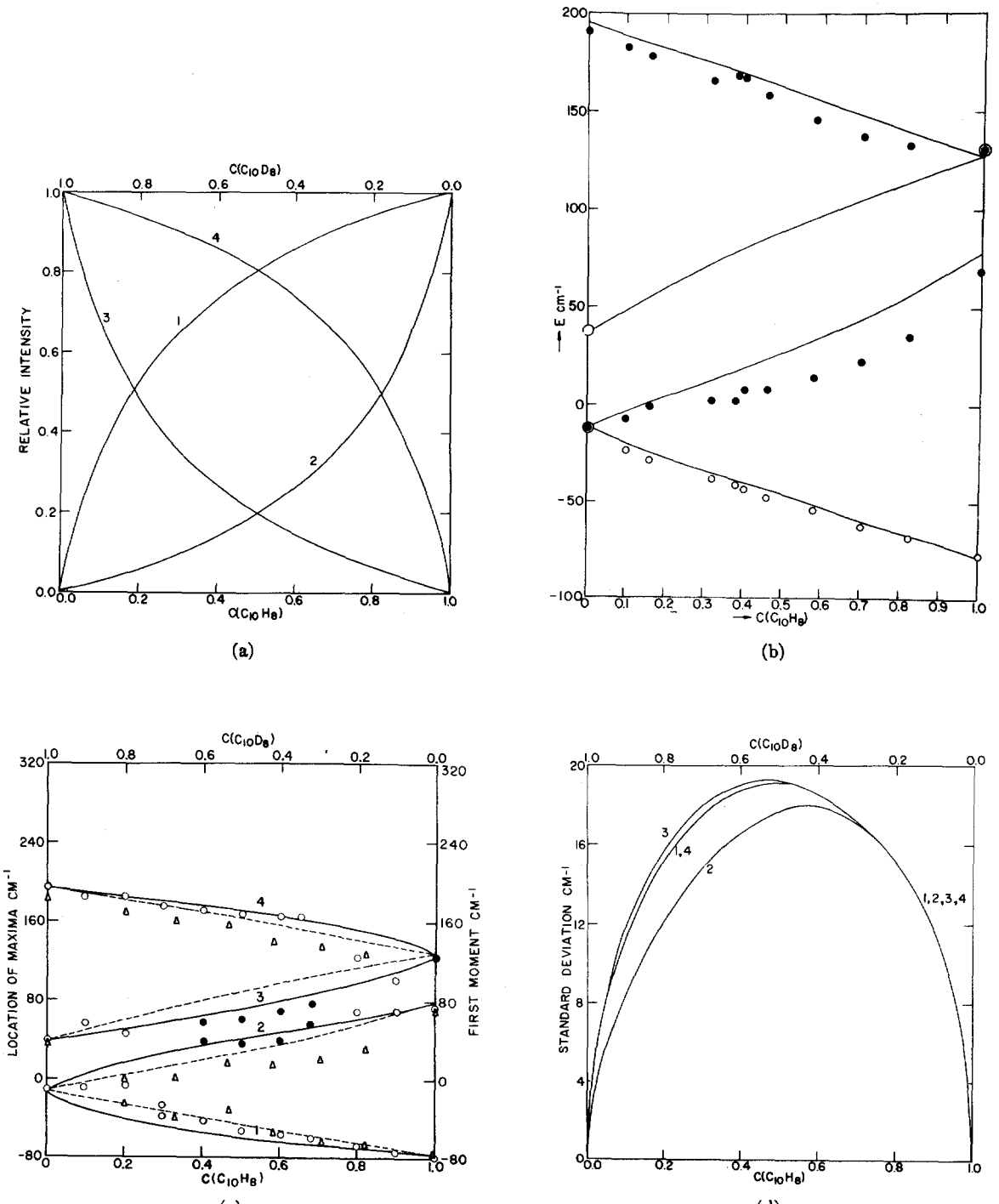

FIG. 16. Optical properties of $C_{10}H_8/C_{10}D_8$ mixed crystals ($\Delta = 115$ cm^{-1}). 1, lower *ac* polarized band; 2, lower *b* polarized band; 3, higher *ac* polarized band; 4, higher *b* polarized band. (a) Relative intensities of absorption bands. (b) First moment of absorption band. The points represent the experimental result of Sheka (Ref. 1): ○, *ac* polarization; ●, *b* polarization. (c) Location of maximum (solid curve) and first moment of absorption band (dashed curve). The points represent the experimental data of Hong and Robinson (Ref. 9): ○, strong optical lines; ●, estimated optical lines. The triangles △ represent Sheka's results (Ref. 1). (d) The width of the absorption bands.

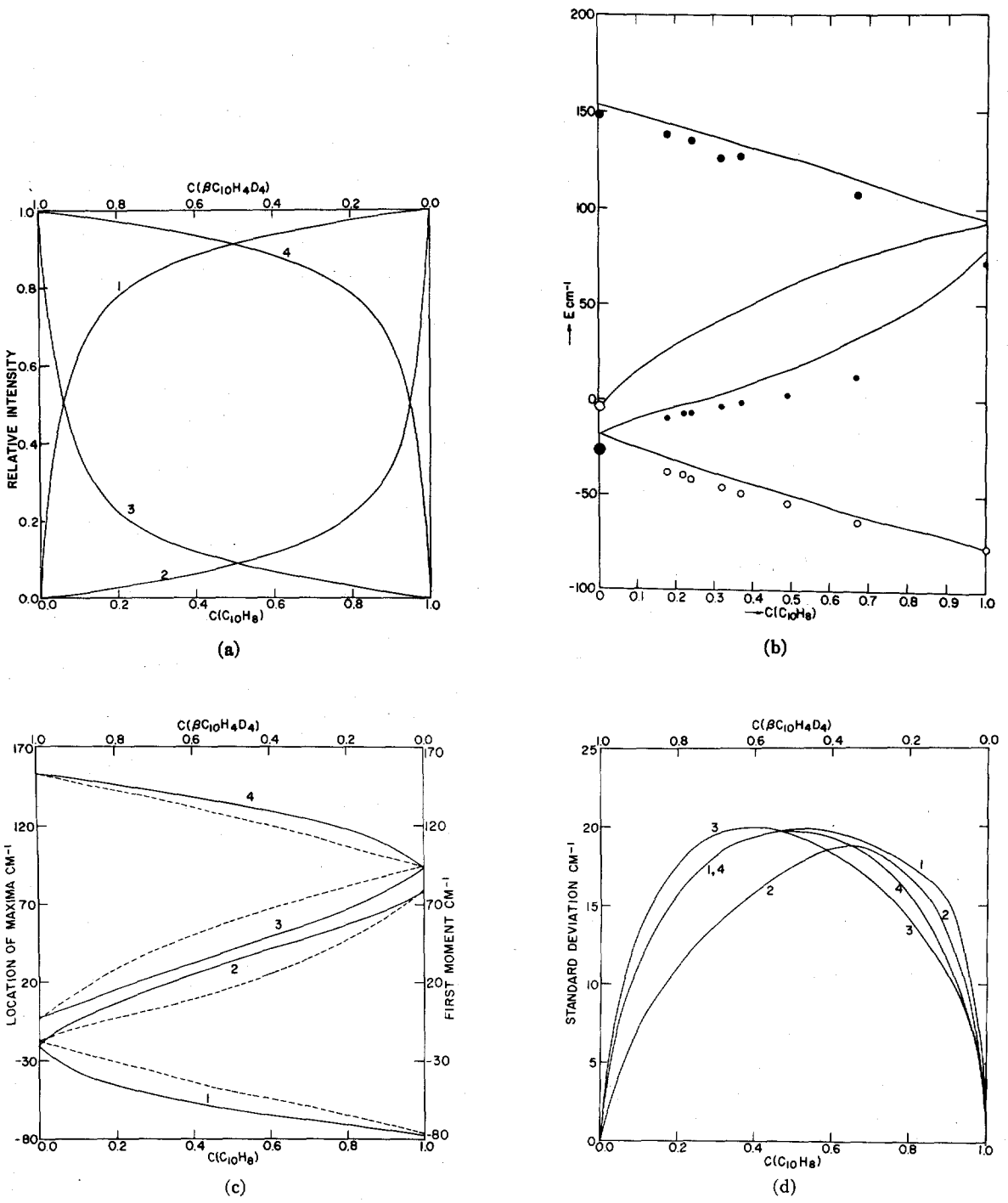

FIG. 17. Optical properties of $C_{10}H_8/\beta$-$C_{10}H_4D_4$ mixed crystals ($\Delta = 74$ cm^{-1}). 1,3, *ac* polarized components. (a) Relative intensities. (b) First moment of absorption band (solid curve). The experimental results of Sheka (Ref. 1) are indicated by dots. ○, *ac* polarization; ●, *b* polarization. (c) Location of band maximum (solid curve) and the first moment (dashed curve). (d) Widths of absorption bands.

integrated intensity, the first moment of the absorption band, the location of the band maximum, and the bandwidth, V, for several binary isotopically mixed naphthalene crystals. The theoretical energetic data are compared with the available experimental data of Sheka and of Hong and Robinson.[9] From the theoretical point of view we infer the following:

(a) The CPA results for the relative intensities in the persistence case ($C_{10}H_8/C_{10}D_8$ and $C_{10}H_8/\beta$-

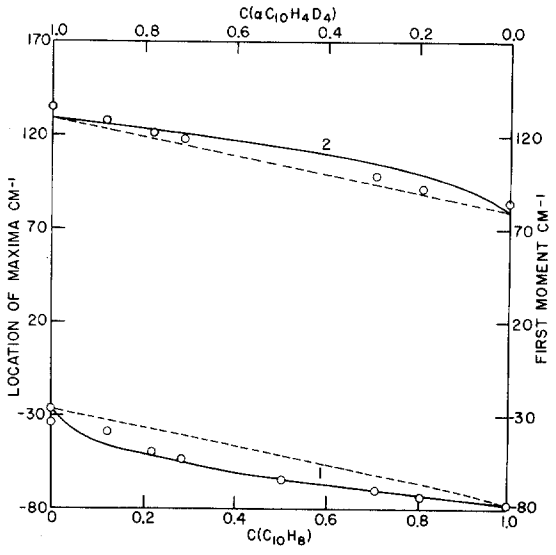

(a)

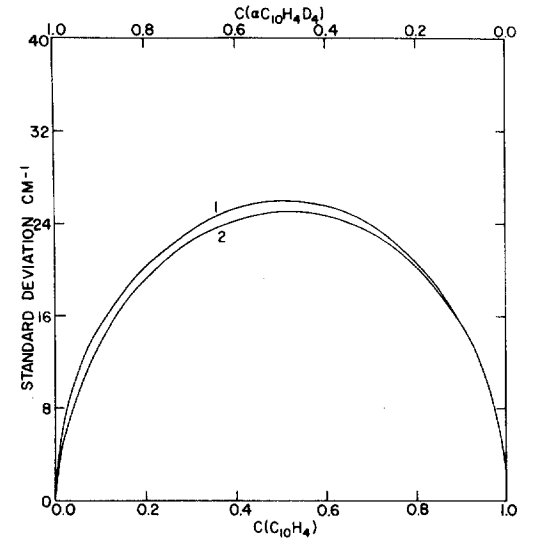

(b)

FIG. 18. Optical properties of $C_{10}H_8/\alpha$-$C_{10}H_4D_4$ ($\Delta=54$ cm^{-1}). 1, *ac* polarized component; 2, *b* polarized component. (a) Location of band maximum (solid line) and first moment (dashed line). The dots represent the experimental results of Hong and Robinson (Ref. 9). (b) Optical bandwidths.

$C_{10}H_4D_4$) concur with the approximate results of the moment expansion method (Eq. II.18)), indicating that the two external absorption bands (at the bottom of the lower band and at the top of the higher band of the density of states) are enhanced relative to the two internal absorption bands. In the case of $C_{10}H_8/\beta$-$C_{10}H_4D_4$ ($\Delta=74$ cm^{-1}) the deviations of the CPA result from the relation (II.18) are quite marked indicating even a larger enhancement effect. In the amalgamation limit, the intensities given by (II.21) correspond to the virtual crystal excited states.

(b) The gross features of the concentration dependence of the first moments of the four absorption bands follow Eq. (II.19) in the separated bands case. In the amalgamation limit the linear concentration dependence (II.22) is rigorously obeyed, for the two absorption bands.

(c) The widths of the four absorption bands in the persistence case are close to the approximate relation (II.23). In the amalgamation limit the exact relation (II.23) is satisfied.

Turning now to the comparison of the CPA results with the available experimental data we note the following:

(a) The experimental data of Sheka[1] for $C_{10}H_8/C_{10}D_8$ and for $C_{10}H_8/\beta$-$C_{10}D_4H_4$ are in reasonable agreement with the calculated first moments of the absorption bands [see Figs. 16(b) and 17(b)]. These results are by no means accurate as the relative concentrations were not directly determined; however, the agreement is rather encouraging.

(b) The experimental data of Hong and Robinson[9] for the $C_{10}H_8/C_{10}D_8$ system [see Fig. 16(c)] are in somewhat better agreement with the location of the absorption band; however, the fitting is not perfect in both cases.

(c) The experimental data of Hong and Robinson[9] in the amalgamation limit for $C_{10}H_8/\alpha$-$C_{10}D_4H_4$ and for $C_{10}H_8/\alpha$-$C_{10}H_7D$ (see Figs. 17 and 18) are in good agreement with the location of the band maximum and with the first moment of the absorption band.

The comparison of the CPA results with experiment is hampered by two difficulties. In the first place, as

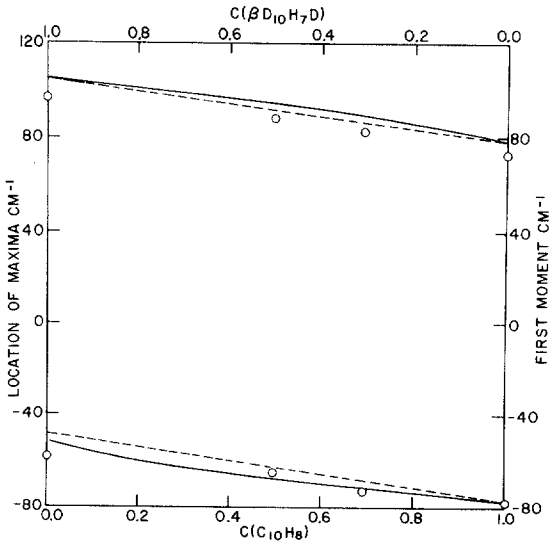

FIG. 19. Optical properties of $C_{10}H_8/\beta$-$C_{10}H_7D$ ($\Delta=26$ cm^{-1}). 1, *ac* polarized component; 2, *b* polarized component. Location of band maximum (solid line) and of the first moment (dashed line). Experimental points from Ref. 9.

pointed out by Hong and Robinson,[9] at low concentrations (below the percolation concentration) the role of impurity clusters may be of considerable importance. Second, the present calculations disregard the role of phonon scattering and attribute the entire optical bandwidth to impurity scattering. In a real crystal the experimentally observed line shape should result as a convolution of the line shape due to lattice vibrations and the strongly asymmetric line shape due to impurity scatterings resulting in the shift of the band maximum. It is therefore unclear at present whether the location of the optical absorption bands in the real mixed crystal will be better approximated by the band maximum or by the first moment of the rigid nonvibrating model system.

We would like to report some results based on the CPA for tertiary isotopically mixed naphthalene crystals. In Figs. 20–24 we display typical data for the density of states and for the optical properties at equal concentrations of the three components. The general features of these results can be summarized as follows:

(a) When a virtual crystal, say, $C_{10}H_8/\alpha$-$C_{10}H_7D$

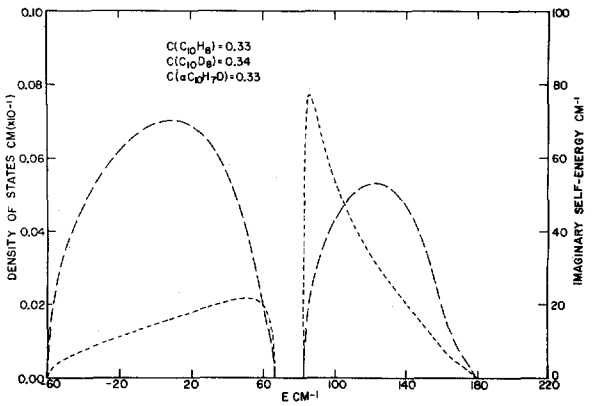

(a)

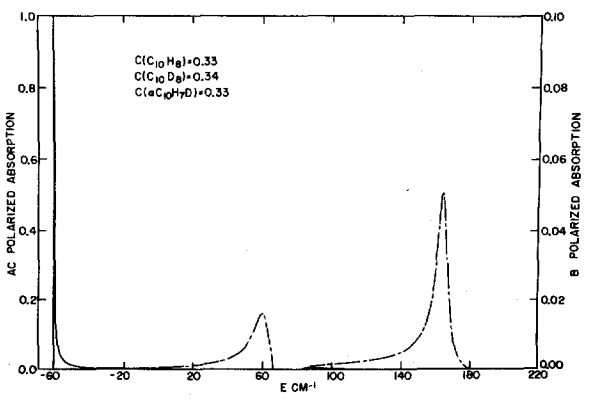

(b)

FIG. 20. Level distribution and optical properties of a tertiary $C_{10}H_8/C_{10}D_8/\alpha$-$C_{10}H_7D$ mixture. (a) Imaginary self-energy (- - -) and density of states (— — —). (b) *ac* polarized (—) and *b* polarized (- - -) optical bands.

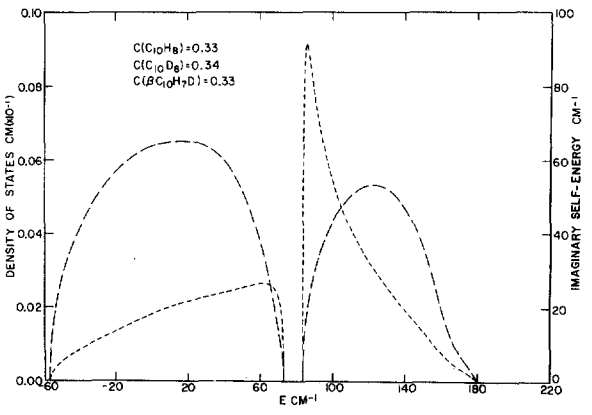

(a)

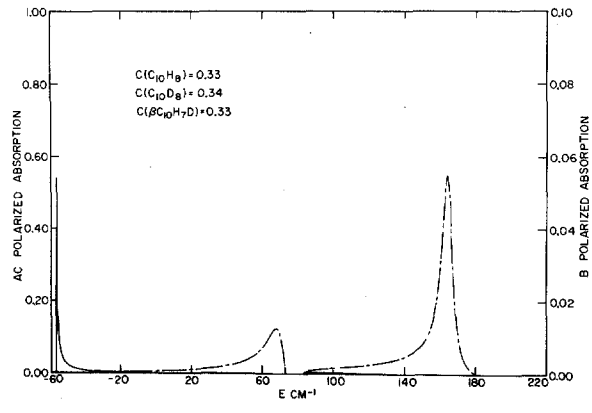

(b)

FIG. 21. Level distribution and optical properties of a tertiary $C_{10}H_8/C_{10}D_8/\beta$-$C_{10}H_7D$ mixture. (a) Imaginary self-energy (- - -) and density of states (— — —). (b) *ac* polarized (—) and *b* polarized (- - -) optical bands.

($\Delta_1 = 14$ cm^{-1}) is relatively strongly perturbed by $C_{10}D_8$($\Delta_2 = 115$ cm^{-1}), a bandgap results in the density of states (see Fig. 20). In this case four absorption bands are exhibited, and the inner *ac* polarized band is appreciably broadened and weakened.

(b) When the perturbation strength Δ_1 is increased while still two components yield a virtual crystal while Δ_2 is kept constant (so that still $\Delta_1 < \Delta_2$), the bandgap closes (see Figs. 21 and 22). In this case four intensity distributions are exhibited in the absorption spectrum, and the broadening and weakening of the two inner bands is pronounced. The same behavior is of course exhibited by the symmetrical case (Fig. 23).

(c) When $\Delta_1 \sim \Delta_2(\mu_2^0)^{1/2}$, two incipient bandgaps are observed in the tertiary mixture (see Figs. 22 and 24). In this case, two pronounced intensity distributions are observed at the band edges, while in the middle of the band weak and broad modulations of these bands are predicted.

The major conclusion that we can draw from this qualitative discussion is that in a tertiary mixed

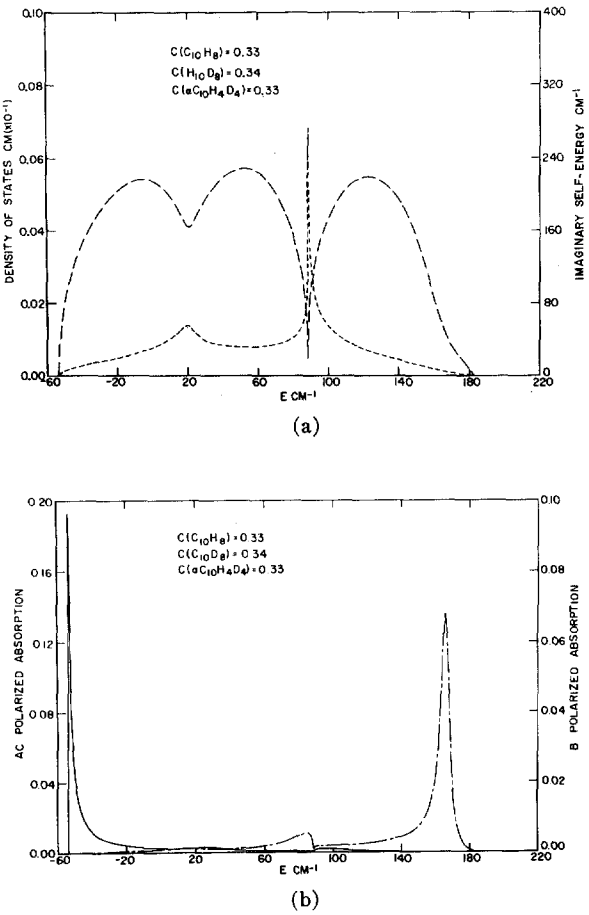

FIG. 22. Level distribution and optical properties of a tertiary $C_{10}H_8/C_{10}D_8/\alpha$-$C_{10}H_4D_4$ mixture. (a) Imaginary self-energy (- - -) and density of states (— — —). (b) *ac* polarized (—) and *b* polarized (- - -) optical bands.

crystal disorder scattering is enhanced relative to the binary system. The middle bands are expected to be considerably weakened and appreciably broadened. These conclusions concur with the available experimental data of Sheka.[1]

VIII. THE LOWEST EXCITED SINGLET STATE OF HEAVILY DOPED CRYSTALLINE BENZENE

Broude and Kochubei[2] studied the optical properties of C_6H_6/C_6D_6 and of C_6H_6/C_6H_5D mixed crystals. Their main experimental results[2] can be summarized as follows:

(a) The location of the absorption band maxima of the low energy *a* and the *b* (or *c*) polarized components in C_6H_6/C_6D exhibits a nearly linear concentration dependence.

(b) In C_6H_6/C_6H_5D mixtures four absorption bands were identified exhibiting marked deviations from a linear concentration dependence.

(c) The intensities of the four Davydov components observed in C_6H_6/C_6D_6 exhibit a linear concentration dependence.

(d) The C_6H_6/C_6H_5D system exhibits a considerable intensity enhancement of the low *a* polarized component, while the higher intensity *a* polarized component is simultaneously decreased. The relative intensities of the two *b*/*c* components is approximately linear with the concentration.

Broude and Kochubei[2] have analyzed their results in terms of the Broude–Rashba scheme,[3] which is applicable only in the atomic limit. We have attempted to apply the CPA to this problem. The pure crystal density of states was adopted from Colson's[21] work and is characterized by the second moment $\mu_2^0 = 110$ cm^{-1} and $W = 60$ cm^{-1}. The positions of the three allowed Davydov components in the pure crystal are[21] $t_1 = -35$ cm^{-1} (*a* polarized), $t_2 = +4$ cm^{-1} (*b* or *c* polarized), and $t_3 = +9$ cm^{-1} (*c* or *b* polarized). The fourth symmetry forbidden *Au* component is located at $t_4 = +25$ cm^{-1}. The relevant perturbation strengths[21,20] are $\Delta = 200$ cm^{-1}, for C_6H_6/C_6D_6 and $\Delta = 35$ cm^{-1} for C_6H_6/C_6H_5D.

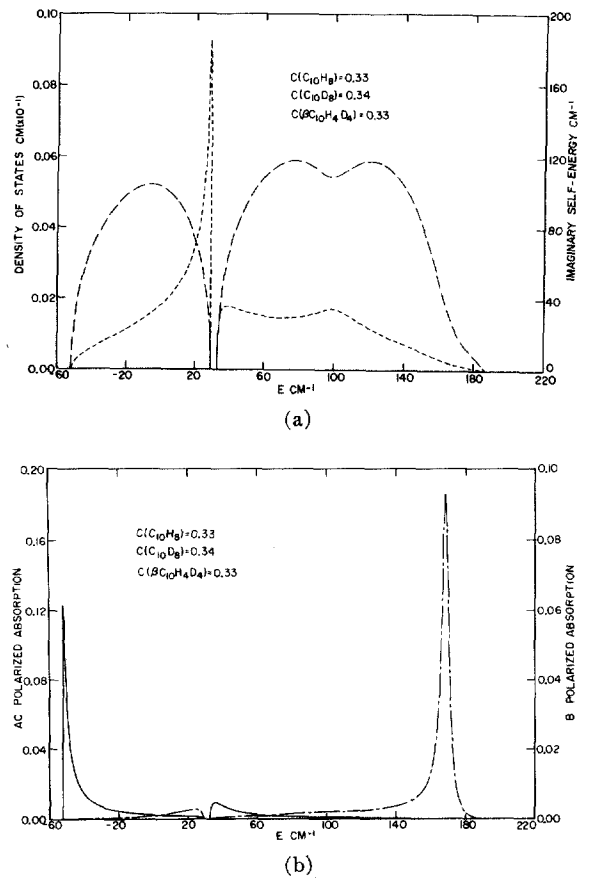

FIG. 23. Level distribution and optical properties of a tertiary $C_{10}H_8/C_{10}D_8/\beta$-$C_{10}H_4D_4$ mixture. (a) Imaginary self-energy (- - -) and density of states (— — —). (b) *ac* polarized (—) and *b* polarized (- - -) optical bands.

For the C_6H_6/C_6D_6 system, $\Delta/W \gg 1$, so that the situation corresponds to separated bands and the optical properties can be adequately expressed by Eqs. (II.18) (II.19), and (II.20) neglecting terms of the order t_j/Δ and μ_2^0/Δ^2. As expected, the CPA calculations yield the same results, whereupon the simple relations result for this case,

$$A^\alpha(j) = |m(j)|^2 C_A, \qquad A^\beta(j) = |m(j)|^2 C_B; \tag{VIII.1}$$

$$E_c^\alpha(j) = \epsilon_A + C_A t_j, \qquad E_c^\beta(j) = \epsilon_B + C_B t_j, \tag{VIII.2}$$

where $\epsilon_i = \Delta\epsilon_i' + D'$. The predicted linear concentration dependence of the integrated intensities [Eq. (VIII.1)] is in good agreement with the experimental results of Broude.[2] On the other hand, the concentration dependence of the positions of the lower a and b/c components predicted from Eq. (VIII.2) exhibits a marked deviation from the experimental results (see Fig. 25). We could have decreased the experimental gas phase value of Δ by ~ 12 cm^{-1} to obtain a better fit at low concentration region of C_6H_6; however, a marked discrepancy between the CPA results and the experimental data is observed. In particular, the energy of the a polarized component decreases with increasing concentration, while Eq. (VIII.2) predicts a slight increase (Fig. 25) for this case.

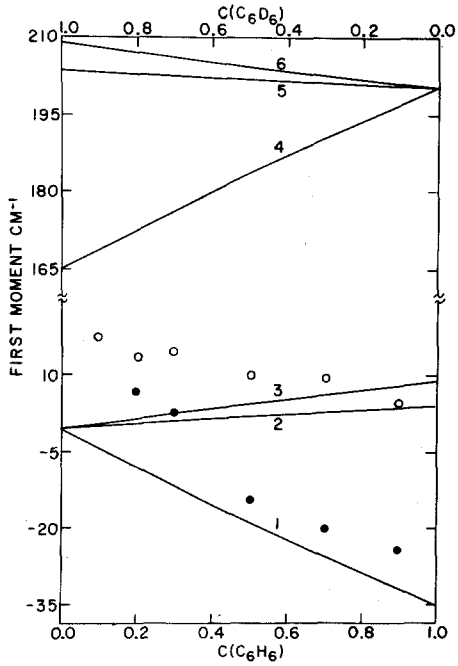

FIG. 25. Location of the band maxima (solid lines) of the six allowed Davydov components of C_6H_6/C_6D_6 as obtained by the CPA. 1 and 4, a polarized; 2 and 5, b/or c polarized; 3 and 6, c/or b polarized. The experimental data of Broude and Kochubei (Ref. 2) for the two lowest components are represented by points: ●, a polarization; ○, b/or c polarization.

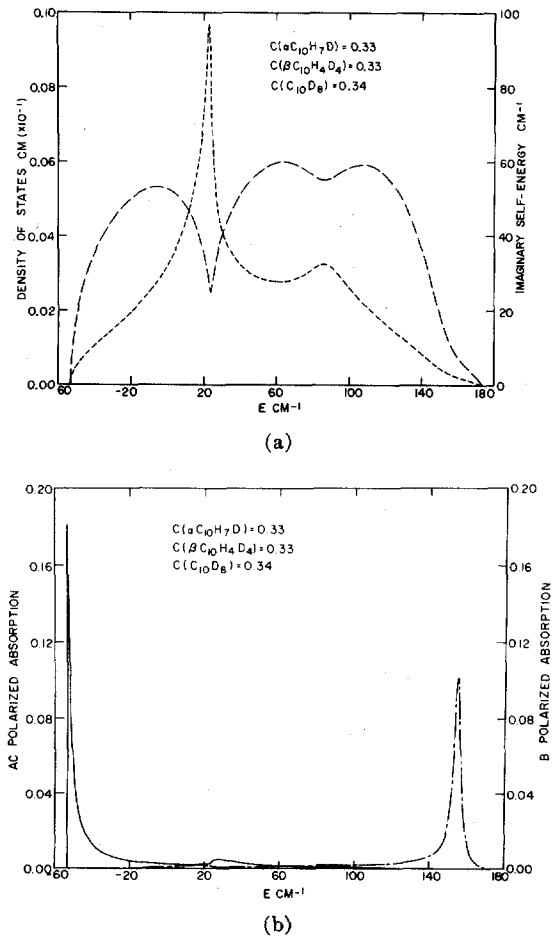

FIG. 24. Level distribution and optical properties of an α-$C_{10}H_7D/\beta$-$C_{10}H_4D_4/C_{10}D_8$ tertiary mixture. (a) Imaginary self-energy (- - -) and density of states (— — —). (b) ac polarized and b polarized (- - -) optical bands.

Turning our attention now to the C_6H_6/C_6H_5D system which corresponds to the persistence case, we display in Fig. 26 the optical properties predicted by the CPA and the experimental data of Broude.[2] The CPA faithfully reproduces the experimental relative intensities [Fig. 26(a)]. As far as the excited energy levels are concerned, it is apparent from Figs. 26(b) and 26(c) that as the b and c components are close relative to their widths only four Davydov components will be experimentally observed in the mixed crystals. However, the position of the absorption bands identified by Broude[2] in this system still exhibit a small but significant systematic departure from the predictions of the simple theory.

The failure of the CPA scheme to account for the excited energy levels of isotopically mixed benzene can be rationalized in terms of the dependence of the environmental shift term D' (which was assumed to be invariant) on the isotopic composition. This point has been raised in the original work of Broude and Kochubei[2] and was also inferred by Colson[21] from his study of low concentration isotopic impurity states

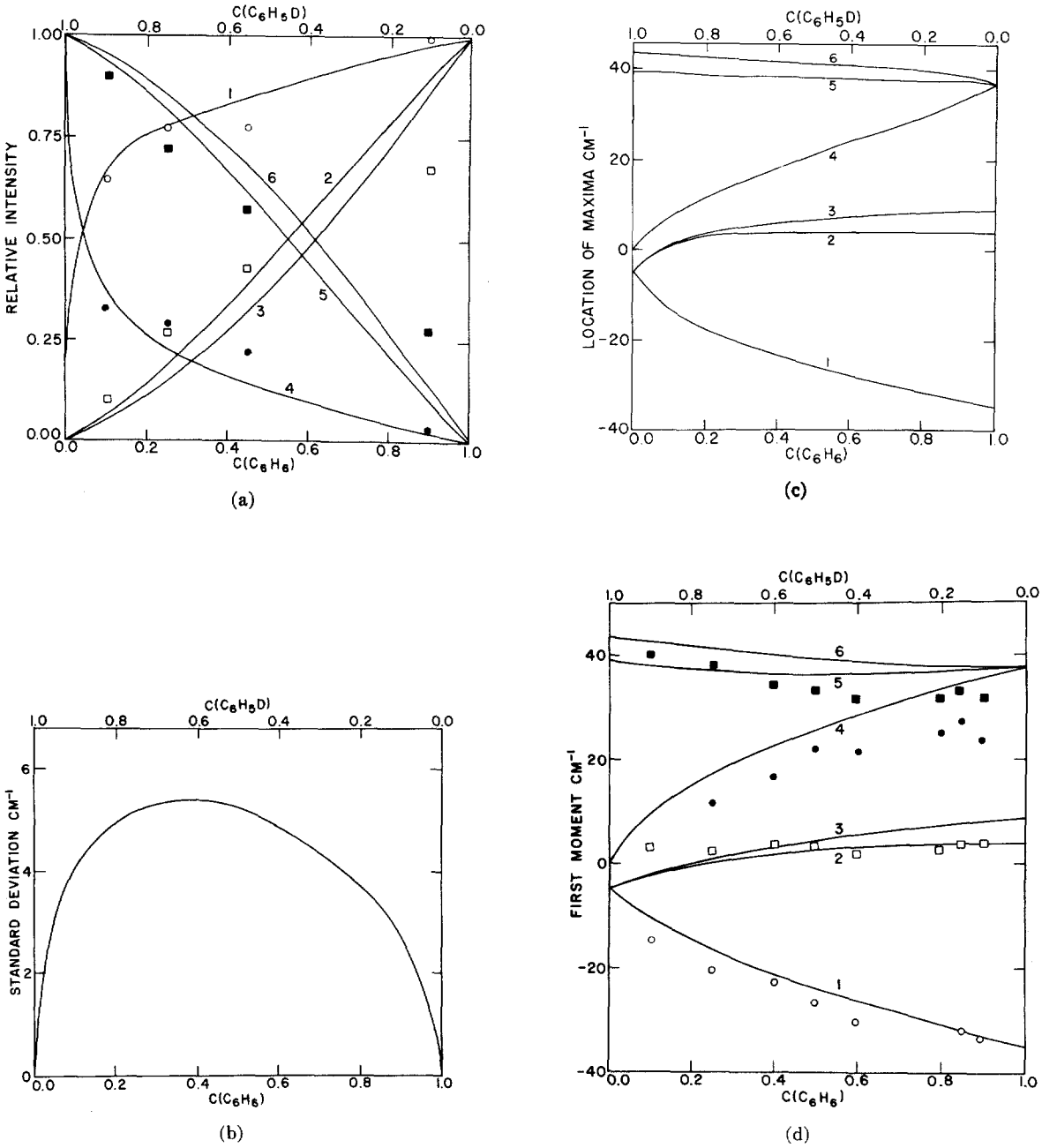

FIG. 26. Optical properties of C_6H_6/C_6H_5D as calculated by the CPA. Calculated curves: 1 and 4, a polarized component; 2 and 5, b/or c polarized component; 3 and 6, c/or b polarized component. Experimental data (Ref. 2): ○, lower a polarized component; □, lower b/or c polarized component; ●, higher a polarized component; ■, higher b/or c polarized component. (a) Relative intensities of absorption bands, as compared with experimental data (Ref. 2). (b) Widths for absorption bands. (c) Location of band maxima. (d) First moment of the absorption bands as compared with experimental data (Ref. 2).

in this system. The D^f term in pure deuterobenzene crystals increases by about 2 cm^{-1} per deuterium atom. This effect is interesting being unique for Frenkel exciton states, and is not encountered for other elementary excitations such as phonons.

A semiquantitative extension of the theoretical scheme to account for the changes in the environmental shift terms can be provided by realizing that these terms appear in the diagonal part of the crystal Hamiltonian (II.1), so that the single site approximation is still adequate. The crystal Hamiltonian for a binary mixture can be rewritten in the form

$$H=\sum_n\sum_\alpha |n\alpha\rangle\epsilon_{n\alpha}\langle n\alpha|+J, \qquad \text{(VIII.3)}$$

where $\epsilon_{n\alpha}=\Delta\epsilon_{n\alpha}{}^f+D_{n\alpha}{}^f$ corresponds to the sum of the

free molecule excitation $\Delta\epsilon_{n\alpha}{}^f$ energy and the (composition dependent) environmental shift term $D_{n\alpha}{}^f$ of the molecule (A or B) located on the site $n\alpha$. In order to generalize the definition of the virtual crystal let us now define four types of environmental shift terms $D_{AA}{}^f$, $D_{BB}{}^f$ $D_{AB}{}^f$, and $D_{BA}{}^f$, where D_{ij} represents the environmental shift of molecule of type i embedded in a crystal of molecules of type j. The virtual crystal Hamiltonian will now include configurational averaging over the pair interactions so that now Eq. (II.1) will be replaced by

$$H_0=\sum_n\sum_\alpha |\, n\alpha\rangle\tilde{\epsilon}_{\rm eff}\langle n\alpha\,|+J, \qquad \text{(VIII.4)}$$

where the effective mean single molecule excitation energy is

$$\tilde{\epsilon}_{\rm eff}(C_A)=C_A\epsilon_A(C_A)+C_B\epsilon_B(C_A) \qquad \text{(VIII.5)}$$

with the concentration dependent diagonal terms

$$\epsilon_A(C_A)=\Delta\epsilon_A{}^f+C_AD_{AA}{}^f+C_BD_{AB}{}^f,$$

$$\epsilon_B(C_A)=\Delta\epsilon_B{}^f+C_BD_{BB}{}^f+C_AD_{BA}{}^f. \qquad \text{(VIII.6)}$$

Now, assuming that the changes in the D^f terms (i.e., $D_{AA}{}^f-D_{BA}{}^f$) are smaller than the width of the exciton band, we can then assert that the major contribution due to the changes in the environmental shift terms can be incorporated in the virtual crystal Hamiltonian, so that we write $H=H_0+H_1$ where H_0 is given by (VIII.4) while H_1 is represented by (II.2a). This approximation rests on the assumption that the changes in the D^f terms do not contribute to the complex self-energy. Now the CPA can be easily extended by replacing the diagonal terms ϵ_A and ϵ_B by the concentration dependent terms $\epsilon_A(C_A)$ and $\epsilon_B(C_B)$ and by replacing $\tilde{\epsilon}$ [Eq. (II.3)] by $\tilde{\epsilon}_{\rm eff}(C_A)$ Eq. [(VIII.3)] in Eqs. (II.18)–(II.20) for the optical properties in the separated bands case, in Eqs. (II.21)–(II.23) for the optical properties in the amalgamation limit, in the general relation (II.26), (II.28) and in the CPA scheme (III.10)–(III.11). This virtual crystal approximation for the changes in the environmental shift terms amounts to a linear extrapolation scheme for the diagonal elements which are now concentration dependent. Several immediate applications of this modified scheme are as follows:

(a) It is immediately apparent that the relative intensities in the separated band limit and also in the persistence case are not markedly affected by the concentration dependence of the environmental shift terms, as Eq. (II.18) reveals that the $A^{\alpha,\beta}(j)$ terms are not dependent on ϵ_A and ϵ_B. Thus it is not surprising that the original CPA scheme accounts well for the experimental intensities in isotopically mixed benzene crystals.

(b) The positions of the optical absorption bands in the separated bands case [Eq. (II.19)] will be dependent, of course, on ϵ_A and ϵ_B, and the modified scheme presented herein is required. For the C_6H_6/C_6D_6 system Eq. (VIII.2) now takes the form

$$E_c{}^\alpha(j)=\Delta\epsilon_A{}^f+D_{AB}{}^f+C_A(t_j+D_{AA}{}^f-D_{AB}{}^f),$$

$$E_c{}^\beta(j)=\Delta\epsilon_B{}^f+D_{BA}{}^f+C_B(t_j+D_{BB}{}^f-D_{BA}{}^f). \qquad \text{(VIII.2')}$$

Colson's[21] data indicate that the environmental shift terms are determined by the nature of the host and $D_{C_6H_6,C_6H_6}{}^f-D_{C_6H_6,C_6D_6}{}^f\sim-12$ cm. Thus the linear dependence of the lowest a and b/c components for C_6H_6/C_6D_6 observed by Broude[2] should be given by $E_c{}^1$ (a polarized) = const $-$ $47C(C_6H_6)$, $E_c{}^1$ (b/c polarized) = const$-8C(C_6H_6)$, and $E_c{}^1(c/b$ polarized) = const$-3C(C_6H_6)$ (all data given in cm^{-1}). The available experimental data (see Fig. 25) are consistent with this modified scheme.

IX. DISCUSSION

In this paper an attempt was made to apply the CPA for the calculation of the density of excited electronic states and of the optical properties for a variety of isotopically substituted crystals. In order to assess the nature of the approximations involved in the present treatment we should consider first the simplified physical model for an isotopically substituted crystal. In the original deviation of the CPA[8] it was explicitly assumed that the environmental shift term D^f and the excitation transfer operator J (see Secs. II and III) are invariant under isotopic substitution. While the excitation transfer matrix elements are transferable from the pure crystal to isotopically mixed crystals, several interesting cases are encountered whereupon the D^f term exhibits a pronounced deuterium effect.[21] Such a situation prevails for isotopically mixed benzene crystals and for s-triazine crystals recently studied by Fisher.[22] In Sec. VIII we have outlined a phenomenological extension of the theoretical scheme, which amends this shortcoming of the basic model. Obviously, for any fixed concentration of the binary mixture the CPA is applicable, provided that the concentration dependence of $\epsilon_A(C_A)$ and of $\epsilon_B(C_B)$ can be extracted from the spectra of the pure crystals A and B and from low concentration impurity states. Obviously, when the pure crystal exciton bandwidth is very narrow, we cannot get away by incorporating the changes in the D^f terms into the virtual crystal Hamiltonian and their correction to the self-energy has to be considered. This problem deserves further study.

Turning now our attention to the CPA we should recall that this approximate scheme rests on two basic assumptions. First, molecule–molecule spatial correlations are disregarded by treating the configurationally averaged mixed crystal. Second, multiple scattering effects are neglected. The second approximation can

be relaxed by the introduction of higher order scattering effects in a systematic manner, as previously done by Soven.[13] It seems that these correction terms are small. The configurational averaging procedure indulging this treatment involves a rather drastic approximation. In particular the effects of clustering will be important at relatively low concentrations below the percolation concentration,[23] which is a three dimensional crystal,[24,25] is around (C_A) percolation $\sim$0.25. while in a linear polymer (C_A) percolation $\sim$1. This is the reason that the CPA results are unreliable for a one dimensional linear chain (see Sec. V). These concentration fluctuation effects will also lead to "tails" in the density of states beyond the shape CPA band limits. The following interesting theoretical problems have to be elucidated:

(a) the nature of deviations from the configurationally averaged crystal, their effects in exhibiting fine structure, and "tails" in the density of states. A cluster expansion new method for the study of the nature of such localized modes has been proposed recently by us, providing a first step in this direction.[23]

(b) the effect of coupling with lattice modes in the substitutionally disordered crystal. As lattice vibrations can be also treated by the CPA it will be interesting to try and establish the effects of coupling between the CPA electronic states and the CPA phonon states in the mixed crystal. In this context it should be noted that the linewidths originating from impurity scattering provide only one contribution to the corresponding experimental quantity which is determined simultaneously by impurity and by phonon scattering.

(c) The transport of electronic excitation energy in substitutionally disordered systems will provide the first step towards the theoretical understanding of energy transfer in disordered systems. In this context we should compare the optical linewidth originating from impurity scattering $Y\sim(\mu_2^0 C_A C_B)^{1/2}$ with the line broadening Γ_p due to phonon scattering. Invoking the very crude assumption that these contributions are additive (although we realize that the compound line shape results from convolution of these two contributions) the total linewidth γ_t is roughly $\gamma_t\sim Y+\Gamma_p$.

The excitation jump (or transfer) time in the strong scattering limit is roughly $\tau_j\sim\hbar\gamma_t/J^2$, where J is a typical intermolecular excitation transfer matrix element (for triplet states and for the lowest singlet in naphthalene and benzene $J\sim$1–10 cm^{-1}). Thus for an equimolar isotopic mixture

$$\tau_j\sim\frac{\hbar[\Gamma_p+(\mu_2^0)^{1/2}/2]}{J^2}=\frac{\hbar}{J}\left(\frac{\Gamma_p+(\mu_2^0)^{1/2}/2}{J}\right).$$

The impurity broadening is $(\mu_2^0)^{1/2}/2\sim$20 cm^{-1} for the lowest singlet state of naphthalene, 5 cm^{-1} for the lowest singlet of benzene, and $\sim$ 2 cm^{-1} for the lowest triplet state of napthalene. These impurity broadening effects are comparable to phonon broadening effects at low temperature of the lowest excited Davydov component in the pure crystal. We thus expect a pronounced role of impurity scattering on the diffusion of electronic excitation in mixed crystals. Unfortunately, low temperature energy transfer experiments are tough.

We hope that the present theoretical study will provide further impetus for experimental work in the optical properties of excited singlet and triplet states of binary and tertiary isotopic mixtures in crystals and polymers, to elucidate the energetics, the line broadening effects and the mechanism of energy migration in substitutionally disordered molecular solids.

APPENDIX: DETAILS OF NUMERICAL CALCULATIONS OF THE SELF-ENERGY

The determination of the self-energy requires the solution of Eq. (III.10) for a two component system and of Eq. (IV.7) for a three component system. Let us define the auxiliary function:

$$F(\sigma(z))=G_I(\sigma(z))-G_{II}(\sigma(z)), \tag{A1}$$

where

$$G_I(\sigma(z))=f^0(z-\tilde{\epsilon}-\sigma(z)) \tag{A2}$$

and f^0 is given by Eq. (III.11). The function G_{II} is

$$G_{II}(\sigma(z))=\sigma(z)/[C_A C_B\Delta^2-\sigma(z)\Delta(C_A-C_B)+(\sigma(z))^2] \tag{A3}$$

for a two component system, and by

$$G_{II}(\sigma(z))=[-Y\pm(Y^2-4XZ)^{1/2}]/2Z \tag{A4}$$

for a three component system. Thus $F(\sigma(z))$ is a complex function of the variable σ with z as a parameter. We have thus to locate the zeros of $F(\sigma)$ in the complex plane for a given parameter z. These zeros yield the desired self-energy $\sigma(z)$. At the first stage of the calculations we employed Newton's method for locating the zeros of the nonlinear equation $F(\sigma)=0$, by the iteration procedure

$$(dF/d\sigma)_{\sigma_0}\delta\sigma-F(\sigma_0)=0 \tag{A5}$$

for a given $\delta\sigma=\sigma-\sigma_0$. This simple numerical procedure is fraught with two difficulties: (a) The iteration procedure (A5) sometimes failed to converge at the band edges. This is rather serious as the optical properties are often determined by the self energy in the vicinity of the band edges. This problem was solved by utilizing a second order iteration procedure

$$\tfrac{1}{2}(d^2F/d\sigma^2)_{\sigma_0}(\delta\sigma)^2-(dF/d\sigma)_{\sigma_0}\delta\sigma+F(\sigma_0)=0. \tag{A6}$$

(b) The numerical integration procedure for evaluating $G_I(\sigma)$ sometimes led to an oscillating behavior of $\sigma(z)$ resulting in an unphysical fine structure in the density of states. Again, this difficulty arose near the band edges where the imaginary component of the self-energy was small. The oscillation was reduced by de-

creasing the integration interval (in the Simpson method). The density of states functions for the two and three dimensional systems were approximated by line segments and each subinterval was integrated analytically, resulting in integrals of the form

$$I(z)=\int_{\alpha}^{\beta}\frac{(ax+b)}{(z-x)}\,dx.$$

The integration intervals were not equally spaced.

Finally, we shall summarize the pertinent expressions required as input data for Eq. (A6):

$$dG_{\mathrm{I}}/d\sigma=\int[\rho^{0}(x)/(y-x)^{2}]dx, \tag{A7}$$

$$d^{2}G_{\mathrm{I}}/d\sigma^{2}=2\int[\rho^{0}(x)/(y-x)^{3}]dx, \tag{A8}$$

where $y=z-C_{\mathrm{B}}\Delta-\sigma$ for a two component system and $y=z-C_{\mathrm{B}}\Delta_{1}-C_{\mathrm{C}}\Delta_{2}-\sigma$ for a three component system. Note that the energy origin has been shifted as in Eq. (V.3).

The derivatives of G_{II} for a two component system are

$$dG_{\mathrm{II}}/d\sigma=(C_{\mathrm{A}}C_{\mathrm{B}}\Delta^{2}+\sigma^{2})/[(C_{\mathrm{A}}C_{\mathrm{B}}\Delta^{2}-(C_{\mathrm{B}}-C_{\mathrm{A}})\Delta\sigma-\sigma^{2})^{2}], \tag{A9}$$

$$d^{2}G_{\mathrm{II}}/d\sigma^{2}=[\sigma C_{\mathrm{A}}C_{\mathrm{B}}\Delta^{2}\sigma+2\sigma^{3}+2(C_{\mathrm{B}}-C_{\mathrm{A}})C_{\mathrm{A}}C_{\mathrm{B}}\Delta^{2}/[(C_{\mathrm{A}}C_{\mathrm{B}}\Delta^{2}-(C_{\mathrm{B}}-C_{\mathrm{A}})\Delta\sigma-\sigma^{2})^{3}]. \tag{A10}$$

For a three component system

$$dG_{\mathrm{II}}/d\sigma=(Q'Z-C'Q)/2Z^{2}, \tag{A11}$$

$$d^{2}G_{\mathrm{II}}/d\sigma^{2}=[Q''Z^{2}-QZC'-2ZC'Q'+2Q(C')^{2}]/2Z^{3} \tag{A12}$$

where

$$Q=-Y\pm(Y^{2}-4XZ)^{1/2}, \tag{A13}$$

$$Q'=-B'\pm[U/(Y^{2}-4XZ)^{1/2}], \tag{A14}$$

$$Q''=B''\pm[U'(Y^{2}-4XZ)-U^{2}]/(Y^{2}-4XZ)^{3/2}, \tag{A15}$$

$$U=YB'-2X(C'+A'Z), \tag{A16}$$

$$U'=YB''+(B')^{2}-2XC''+2A'C', \tag{A17}$$

$$A'=1, \qquad A''=0;$$

$$B'=4\sigma+c, \qquad B''=4;$$

$$C'=3\sigma^{2}+2c\sigma-e-a, \qquad C''=\sigma\sigma+2\sigma. \tag{A18}$$

X, Y, and Z were defined in Eq. (IV.8); a, b, c, d, e were defined in Eq. (IV.9).

The numerical calculations were performed on a CDC 3400 computer at the Computation Centre of the Tel-Aviv University. All the figures presented in this work represent the tracings of the output of the computer plotter without any modifications.

[1] E. F. Sheka, Bull. Acad. Sci. U.S.S.R. Phys. Series **27**, 501 (1963).
[2] V. L. Broude and S. M. Kochubei, Fiz. Tverd. Tela **6**, 354 (1964) [Sov. Phys. Solid State **6**, 285 (1964)].
[3] V. L. Broude and E. I. Rashba, Fiz. Tverd. Tela **3**, 1941 (1961) [Sov. Phys. Solid State **3**, 1415 (1962)].
[4] D. P. Craig and M. R. Philpott, Proc. Roy. Soc. (London) **A290**, 602 (1966).
[5] A. Hernzenberg and A. Modines, Biopolymers **2**, 561 (1964).
[6] O. Onodera and Y. Toyozawa, J. Phys. Soc. Japan **24**, 341 (1967).
[7] K. W. Hong and G. W. Robinson, J. Chem. Phys. **52**, 825 (1970).
[8] J. Hoshen and J. Jortner, Chem. Phys. Letters **5**, 351 (1970).
[9] K. W. Hong and G. W. Robinson, J. Chem. Phys. **54**, 1369 (1971).
[10] J. Hoshen and J. Jortner, J. Chem. Phys. **56**, 933 (1972).
[11] B. Velicky, S. Kirkpatrick and H. Ehrenreich, Phys. Rev. **175**, 747 (1968).
[12] P. Soven, Phys. Rev. **156**, 809 (1967).
[13] P. Soven, Phys. Rev. **178**, 1136 (1969).
[14] G. F. Koster and J. C. Slater, Phys. Rev. **95**, 1167 (1954).
[15] (a) J. Jortner, S. A. Rice, J. L. Katz, and S. I. Choi, J. Chem. Phys. **42**, 309 (1965). (b) B. Sommer and J. Jortner, *ibid.* **50**, 839 (1969).
[16] D. M. Hanson and G. W. Robinson, J. Chem. Phys. **43**, 4174 (1965).
[17] J. Hoshen and J. Jortner (unpublished).
[18] D. M. Hanson, R. Kopelman, and G. W. Robinson, J. Chem. Phys. **48**, 2215 (1968).
[19] D. M. Hanson, R. Kopelman, and G. W. Robinson, J. Chem. Phys. **51**, 212 (1969).
[20] B. Sommer and J. Jortner, J. Chem. Phys. **50**, 822 (1969).
[21] S. D. Colson, J. Chem. Phys. **48**, 3324 (1968).
[22] G. Fischer, "The Variable Trap Problem in Isotopic Mixed Crystals of *s*-Triazine" (to be published).
[23] J. Hoshen and J. Jortner, J. Chem. Phys. **56**, 4138 (1972).
[24] R. J. Elliott and B. R. Heap, Proc. Roy. Soc. (London) **A265**, 264 (1962).
[25] G. S. Rushbrooke and D. J. Morgan, J. Mol. Phys. **4**, 1 (1961).